Carbon Isotope Stratigraphy of the Cambrian System in the Eastern Tarim Basin, China

WANG Huajian, SU Jin, WANG Xiaomei, YE Yuntao, WANG Yu, FANG Yu and ZHANG Shuichang*

Research Institute of Petroleum Exploration & Development, Beijing 100083, China

Abstract: The ultra-deep Cambrian System in the Tarim Basin is an important field for petroleum exploration, while fine division of the Cambrian strata remains controversial. In recent years, carbon isotope stratigraphy of the Cambrian System has been established and widely used. Here, we report an integrated profile of carbonate and organic carbon isotopic values ($\delta^{13}C_{carb}$ and $\delta^{13}C_{org}$) from cuttings of the Tadong2 Well in the eastern Tarim Basin. Three carbon isotope anomalies of BACE, ROECE and SPICE were recognized on the $\delta^{13}C_{carb}$ profile. Three apogees and a nadir on the $\delta^{13}C_{org}$ profile and the onset of ROECE on the $\delta^{13}C_{carb}$ profile were suggested as boundaries of the present four series of the Cambrian System. Suggested boundaries are easily identifiable on the gamma logging profile and is consistent with the previous division scheme, based on biostratigraphic evidence in outcrop sections. Abnormal carbon cycle perturbations and organic carbon burials during the BACE and SPICE events might be related to the reduction and expansion of a huge dissolved organic carbon reservoir in the deep ocean of the ancient Tarim Basin.

Key words: organic carbon, black shale, dissolved organic carbon, BACE, SPICE, stratigraphic division

Citation: Wang et al., 2022. Carbon Isotope Stratigraphy of the Cambrian System in the Eastern Tarim Basin, China. Acta Geologica Sinica (English Edition), 96(4): 1277–1293. DOI: 10.1111/1755-6724.14972

1 Introduction

Huge amounts of oil and gas have been discovered in the ultra-deep Cambrian strata of the Sichuan and Tarim basins in China, with the largest potential contribution being from the lower Cambrian black shales (Zhang and Huang, 2005; Zou et al., 2014). The Cambrian is the first period of the Phanerozoic Eon, the explosion of Cambrian life indicating a revolutionary transition in the evolution of life, from the Proterozoic ecosystem dominated by autotrophic organisms to the Phanerozoic ecosystem, characterized by heterotrophic predators (Zhu et al., 2019; Zhang and Shu, 2021). In the Sichuan Basin and the Yangtze Craton where it is located, both thickness and distribution range of the lower Cambrian black shale are very large, the organic carbon burial mechanism and carbon cycle process having been extensively studied (Ishikawa et al., 2013; Zhang et al., 2020b). The Chengjiang Biota and the Qingjiang Biota, discovered in the Yangtze Craton, record early Cambrian life in shallow water and deep water, respectively (Zhao et al., 2010; Fu et al., 2019). However, in the Tarim Basin, the already discovered lower Cambrian black shale is thin (mostly <30 m) and limited in scope (Zhu et al., 2018). This is related to the unfavourable research conditions for the Cambrian sediments in the Tarim Basin, such as the large burial depth, limited deep drilling cores, poor outcrop exposures, harsh field work environment etc.. Therefore, it is important to use deep drilling cuttings to carry out identification and distribution prediction for the lower Cambrian black shale in the Tarim Basin.

Based on biostratigraphic research, the base of the Terreneuvian, Miaolingian and Furongian in the current quadrant scheme (Terreneuvian, Series 2, Miaolingian and Furongian) of the international Cambrian System has been established (Zhu et al., 2019). However, Cambrian biostratigraphic studies on the Tarim Basin were mainly conducted several decades ago and concentrated in peripheral outcrops, such as the Kuluketage region in the northeast and the Keping region in the northwest (Zhang, 1983; Zhu and Lin, 1983; An and Zhang, 1986; Wang and Zhu, 1988; Zhang, 1990; Zhou and Chen, 1990; Lin et al., 2001; Dong et al., 2009). Due to a limited quantity of drilling cores and cuttings, only a few biostratigraphic studies have been carried out in the area covered (Xiong et al., 2011; Huang et al., 2017). In most cases, rough inference and strata divisions were made, based on lithological features, well logging and seismic stratigraphy (Cai et al., 2014; Yan et al., 2020), which might limit the target accuracy and increase the risk of failure during ultra-deep petroleum exploration.

In recent years, sampling accuracies and data sources for carbon isotopic compositions of carbonate ($\delta^{13}C_{carb}$) and organic carbon ($\delta^{13}C_{org}$) have continued to increase. Variations of paired $\delta^{13}C_{carb}$ and $\delta^{13}C_{org}$ record the changes between the fraction of organic carbon manufactured and preserved through time (Kump and Arthur, 1999), as well as providing clues to trace the redox conditions of the oceanic environment and the origin of the organic carbon (e.g., planktonic algae,

* Corresponding author. E-mail: sczhang@petrochina.com.cn

photosynthetic bacteria or chemoautotrophic bacteria) (Hayes et al., 1999). Obvious $\delta^{13}C_{carb}$ or/and $\delta^{13}C_{org}$ anomalies (negative or positive excursions) are considered as carbon cycle perturbations, which are closely related to a series of oceanic oxic events (OOEs) or oceanic anoxic events (OAEs), as well as biological radiation and/or extinction events (Jenkyns, 2010; Alcott et al., 2019). Therefore, a high-resolution carbon isotope profile is often used as an alternative method in fine stratigraphic division and comparison, especially when the chronostratigraphic and biostratigraphic data are lacking. The currently established and widely-used global Cambrian $\delta^{13}C_{carb}$ standard curve consists of 6 negative excursions (BACE, SHICE, AECE, ROECE, DICE, TOCE) and 4 positive excursions (ZHUCE, CARE, MICE, SPICE) (Fig. 1) (Zhu et al., 2006; Zhu et al., 2019). Limited sample demand and high data reproducibility of $\delta^{13}C$ analysis further act to ensure that carbon isotope stratigraphy has become the method with the most potential to do fine stratigraphic division and comparison in the area covered (Chen et al., 2020).

Herein, we report $\delta^{13}C_{carb}$, $\delta^{13}C_{org}$ and total organic carbon (TOC) values of cuttings within the 5000–4500 m interval of the Tadong2 Well in the eastern Tarim Basin. The three carbon isotope anomalies of BACE, ROECE and SPICE were recognized from the $\delta^{13}C_{carb}$ profile (Fig. 1).

2 Geological Setting

2.1 Tectonic and paleogeographic setting

The Tarim Basin is the largest basin in China, with a crystalline basement formed in the Neoarchean Era and cratonization occurring in the Mesoproterozoic Era (Zhai, 2013). The Tarim Block is a microcraton, but is important in the reconstruction of ancient supercontinents, such as the Columbia, Rodinia, Gondwana and Pangea supercontinents (Meert and Santosh, 2017; Zhao et al., 2018). Almost all models place the Tarim Block at the outer edge of each supercontinent, except the Pangea supercontinent (Zhao et al., 2018), indicating that the Tarim Block might have been evolving independently until the Ordovician Period (Fig. 2a–b). During the Cryogenian and Ediacaran periods, along with the breakup of the Rodinia supercontinent and the evolution of the Paleo-Tethys Ocean, the Tarim Block underwent strong rifting and received deposition in the north and southwest (Bai et al., 2020; Ren et al., 2020). By the early Cambrian, the Tarim Block might have evolved into a passive continental margin and developed synsedimentary faults in the North Depression (Guan et al., 2019) (Fig. 2c). Throughout most of the duration of the Cambrian and Ordovician periods, the Tarim Block was a small isolated block surrounded by deep-ocean basins, independent from the eastern and western parts of the Gondwana

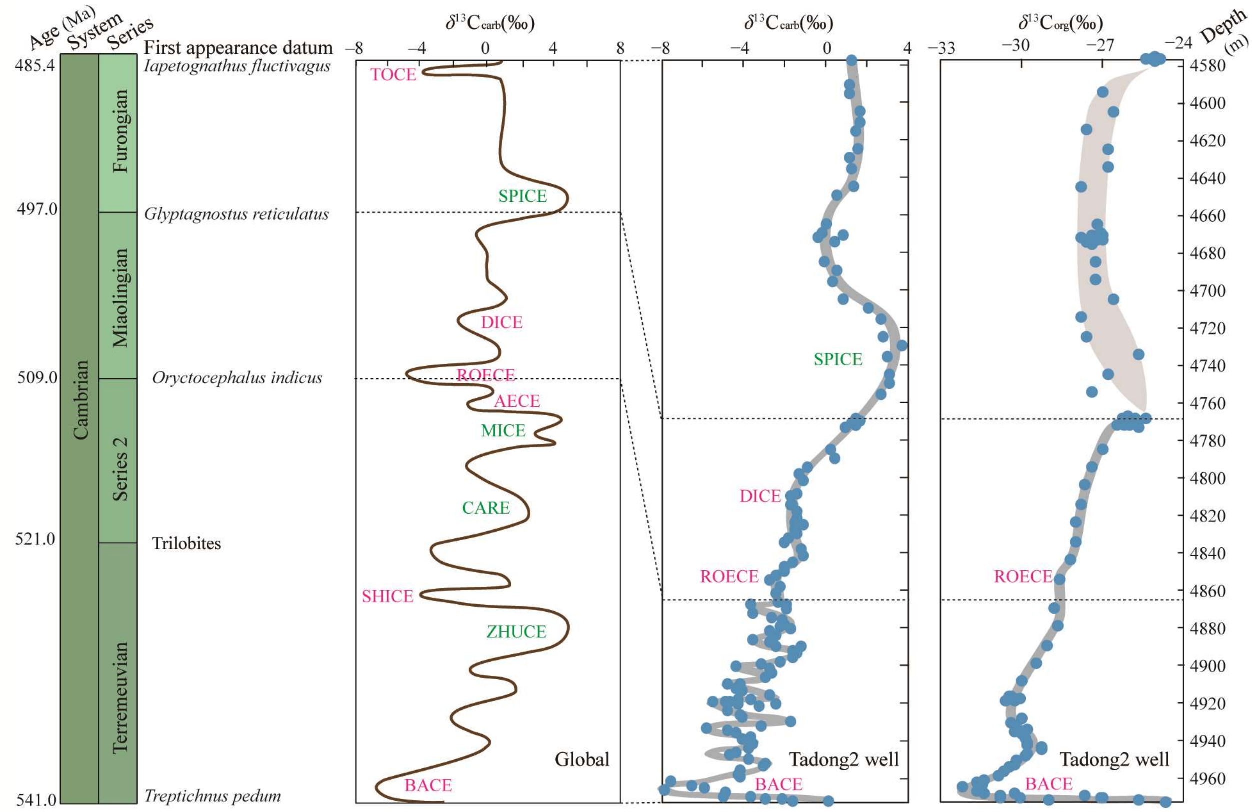

Fig. 1. Global Cambrian chronostratigraphy, carbon isotope stratigraphy (Zhu et al., 2019) and $\delta^{13}C_{carb}$ and $\delta^{13}C_{org}$ profiles of the Tadong2 Well in the Tarim Basin (this paper).

BACE = Basal Cambrian Carbon isotope Excursion; ZHUCE = ZHUjiaqing Carbon isotope Excursion; SHICE = SHIyantou Carbon isotope Excursion; CARE = Cambrian Arthropod Radiation isotope Excursion; MICE = MIngxinsi Carbon isotope Excursion; AECE = Archaeocyathid Extinction Carbon isotope Excursion; ROECE = Redlichiid-Olenellid Extinction Carbon isotope Excursion; DICE = DrumIan Carbon isotope Excursion; TOCE = Top of Cambrian Excursion.

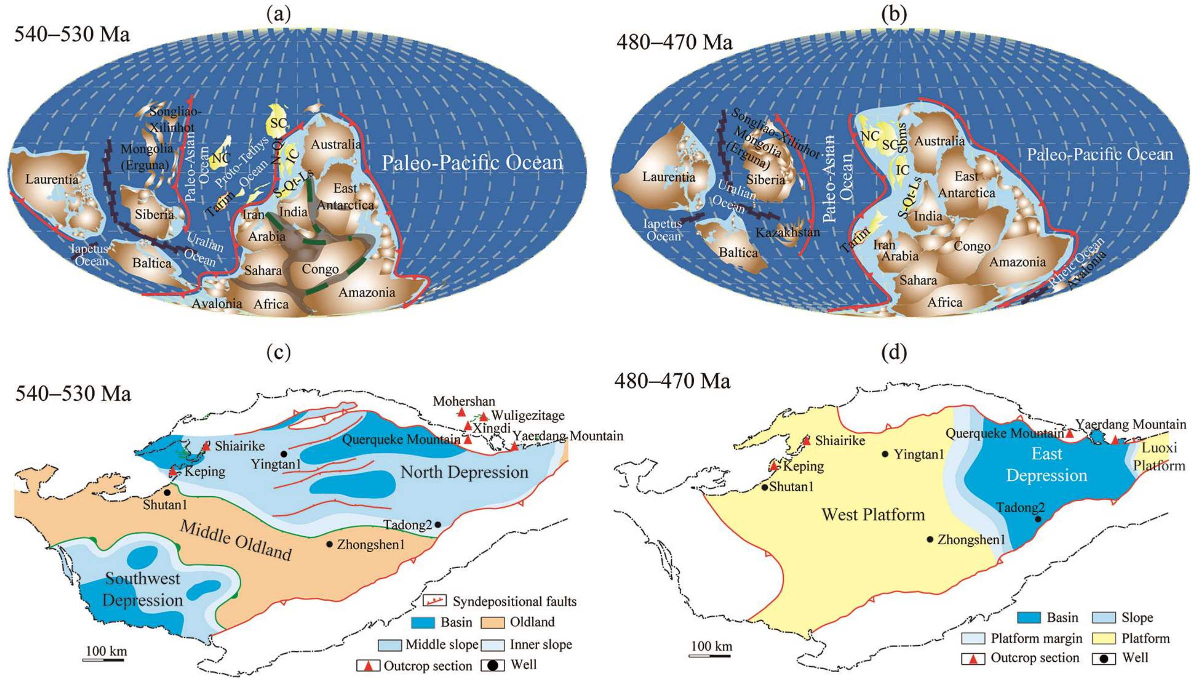

Fig. 2. Paleo-plate locations (a, b) and paleogeographic features (c, d) of the Tarim Basin during the early Cambrian (540–530 Ma) and the Early Ordovician (480–470 Ma).
(a) and (b) were cited from Zhao et al. (2018); (c) and (d) were modified from Guan et al. (2019) and Zhao et al. (2011), respectively.

supercontinent (Fig. 2a–b). Following the global transgression and the assembly of the Gondwana supercontinent in the Cambrian Period, the Tarim Block gradually moved to the mid latitudes of the southern hemisphere from the lower latitudes of the tropical region, approaching the western side of the East Gondwana supercontinent (Zhao et al., 2018) (Fig. 2b). The Middle Oldland of the Tarim Block gradually submerged to form a large-scale platform named the West Platform (Zhao et al., 2011). Between the West Platform and the Luoxi Platform, there was a depression named the East Depression (Zhao et al., 2011) (Fig. 2d).

2.2 Lithostratigraphic setting

In the western Tarim Basin, the Cambrian System is divided into (from bottom to top) the Yurtus, Xiaoerbulake, Wusonger, Shayilik, Awatag and Xiaqiulitag formations (Zhu et al., 2019). The black shale of the Yurtus Formation, with a thickness of less than 20 m, was deposited in the early Cambrian (Zhu et al., 2018). Parallel unconformities between the Yurtus Formation with the underlying Ediacaran Chigebrak Formation and the overlying Cambrian Xiaoerbulake Formation have been found in the Keping and Shiairike outcrop sections (Zhang et al., 2020c; Zhu et al., 2021c). The upwards Xiaoerbulake, Wusonger, Shayilik, Awatag and Xiaqiulitag formations are continuous depositions and dominated by dolostone. According to carbon isotope stratigraphy, Zhang et al., (2020c) proposed a long-term sedimentary discontinuity between the Yurtus and Xiaoerbulake formations. Therefore, the Cambrian record in the western Tarim Basin may be incomplete.

In the eastern Tarim Basin, the Cambrian System is divided into (from bottom to top) the Xishanblaq, Xidashan, Mohershan and Tuershaketage formations (Cai et al., 2014). Among them, the Mohershan Formation used here contains the Mohershan and Chuanxingshan formations mentioned in Zhang (1990) and Zhu et al. (2021c). In most places, the chert at the base of the Xishanblaq Formation unconformably overlies the glaciogenic Hankalchough Formation resulting from probable Ediacaran glaciation. The Xishanblaq Formation and the upwards Xidashan, Mohershan and Tuershaketage formations are continuous depositions with gradual variations from black shale to argillaceous limestone and then to limestone. The Ordovician Heituao Formation overlying the Tuershaketage Formation is dominated by black shale, with a limited distribution range in the eastern Tarim Basin.

2.3 Biostratigraphic setting

Biostratigraphic studies of the eastern Tarim Basin were mainly from outcrop sections, such as Mohershan, Yaerdang Mountain, Querqueke Mountain, Xingdi and Wuligezitage (Fig. 2c). Small shelly spherical fossils, acrotretid brachiopods *gen. et sp. indet. B* and the *Asteridium*-*Heliosphaeridium*-*Comasphaeridium* (AHC) acritarch assemblage appear in the chert-phosphorite unit of the Xishanblaq Formation in the Mohershan section and Yurtus Formation in the Aksu area, corresponding to the first small shelly zone of the Meishucunian Stage in South China (Yao et al., 2005; Zhu, 2007; Dong et al., 2009), indicating that the lower chert is very close to the Cambrian base (Fig. 3). The trilobite zones of *Metaredlichioides*-*Chengkouia*, *Tianshano-cephalus* and *Arthricocephalus*-*Changaspis*, Pleospongia of *Protospongia*, brachiopods of

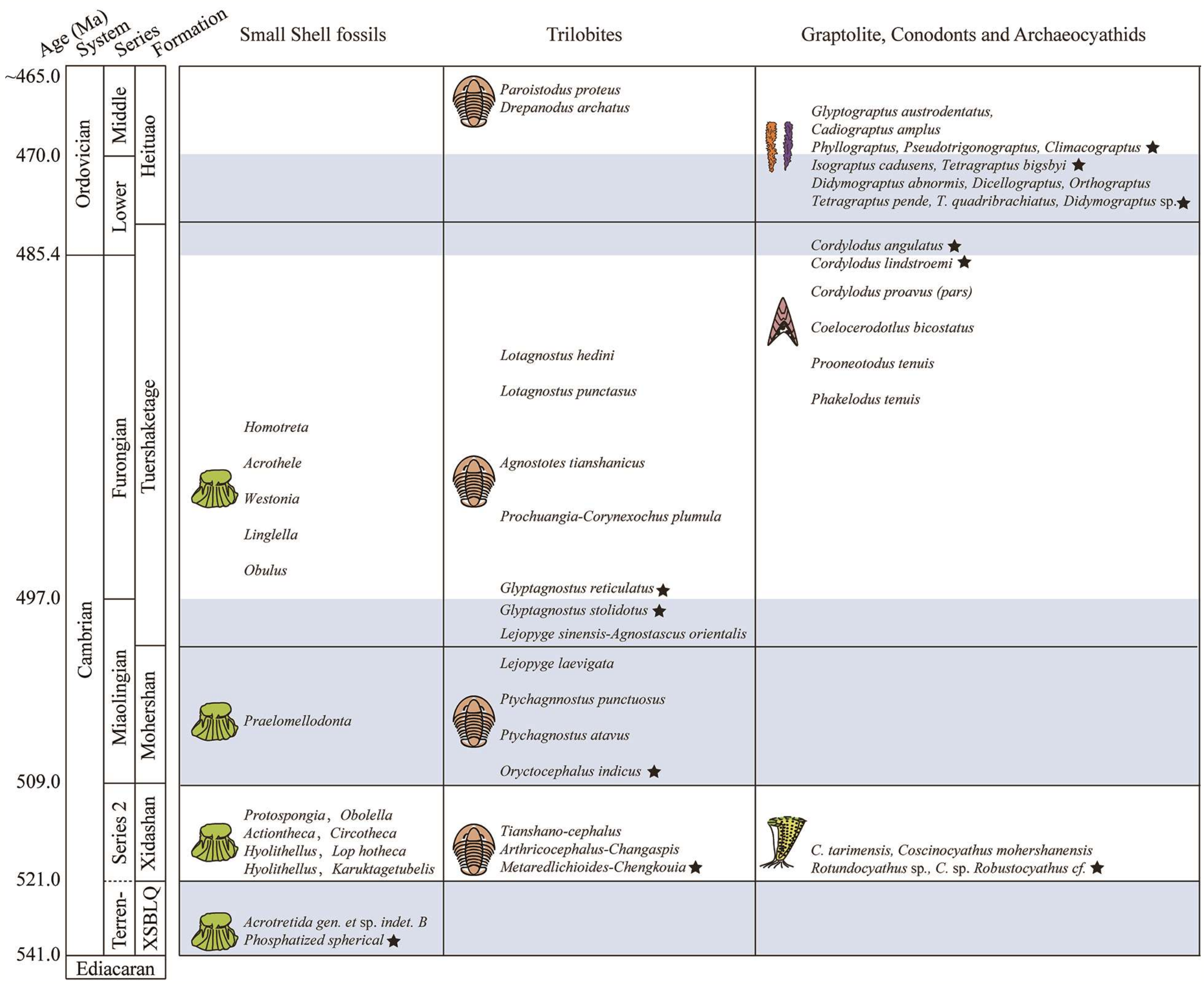

Fig. 3. Paleontological stratigraphy of the Cambrian and Ordovician in the eastern Tarim Basin.
Terren-, Terreneuvian; XSBLQ, Xishanblaq. Pentagrams represent key biological zones in stratigraphic division. Data sources, Zhang, 1983; Zhu and Lin, 1983; An and Zhang, 1986; Zhang, 1990; Du et al., 2004; Yang, 1994; Lin et al., 2001; Zhu, 2007; Xiong et al., 2011; Zhu et al., 2019.

Obolella sp. and archaeocyathids of *Coscinocyathus mohershanensis*, *C. tarimensis*, *Rotundocyathus* sp., *Robustocyathus* cf. *kruzini* found from the Xidashan Formation in the Mohershan section (Zhang, 1983; Zhu and Lin, 1983), suggest an isochronous deposition of the Xidashan Formation and Series 2 (Fig. 3). The Global Stratotype Section and Point (GSSP) of the Miaolingian and Furongian was marked by the first appearance datum (FAD) of the trilobite zones of *Oryctocephalus indicus* and *Glyptagnostus reticulatus*, respectively (Peng et al., 2004). In the Kuluketage region, these two trilobite zones have been found at the base of the Mohershan Formation and the bottom of the Tuershaketage Formation, respectively (An and Zhang, 1986; Zhang, 1990). Therefore, the base of the Mohershan Formation may be consistent with that of the Miaolingian Series, while the base of the Tuershaketage Formation is below that of the Furongian Series (Fig. 3). In the Querqueke Mountain section, some other trilobites with FADs in the Furongian, such as *Proceratopyge* sp., *Pseudagnostus* sp., *Lotagnostus* sp., *Charchaqia* sp., *Hedinaspis* sp. have also been found from the Tuershaketage Formation (An and Zhang, 1986).

The GSSP of the Cambrian–Ordovician boundary was marked by the FAD of the conodont zone of *Iapetognothus fluctivagus* in the Green Point section, western Newfoundland, Canada (Cooper et al., 2001). In the Yaerdang Mountain section, the conodont zones of *Cordylodus proavus* (pars), *Cordylodus lindstroemi* and *Cordylodus angulatus* have been found from the top of the Tuershaketage Formation, while *Iapetognothus fluctivagus* has not been found (Lin et al., 2001). As the FAD of *Iapetognathus fluctivagusis* lies between the FADs of *Cordylodus lindstroemi* and *Cordylodus angulatus* in the Green Point GSSP section (Cooper et al., 2001) and the Lawson Cove candidate section of Utah, USA (Miller et al., 2006), the Cambrian–Ordovician boundary should be placed at the top of the Tuershaketage Formation, between the conodont zones of *Cordylodus lindstroemi* and *Cordylodus angulatus* (Fig. 3). In other words, the Cambrian–Ordovician boundary should be lower than the apex of the Tuershaketage Formation. The Heituao Formation is rich in graptolites. In the Wuligezitage section, graptolite zones of *Tetragraptus bigsbyi*, *Didymograptus abnormis* and *Isograptus cadusens* have been found from the middle of the Heituao Formation, above the graptolite zones of *Tetragraptuspende*, *T. quadribrachiatus*, and *Didymograptus* sp. at the bottom and below the graptolite zones of *Cadiograptus amplus*, *Glyptograptus austrodentatus* at the top (Yang, 1994). For the FAD of *Tetragraptus bigsbyi* in the Lower Ordovician (Chen et al., 2009), the Heituao Formation is inferred to be Lower–Middle Ordovician (Fig. 3).

2.4 The Tadong2 Well

The Tadong2 is a deep well with a depth of over 5000 m (Zhang et al., 2004). This well was drilled through the entirety of the Ordovician and Cambrian sediments and reached the Ediacaran sediment. In the Tadong2 Well, the Ediacaran Hankalchough Formation is mainly composed of diamictite, shale and dolostone, with a thickness of about 99 m. Dolostone at the top of the Hankalchough Formation might be the 'cap dolostone' after the last Ediacaran glaciation (Xiao et al., 2004). Differing from the outcrop sections in the Kuluketage region, the basal Xishanblaq Formation of the Tadong2 section is black shale without cherts. Based on gamma (GR) values and lithostratigraphic features, the depth ranges of the Xishanblaq, Xidashan, Mohershan, Tuershaketage and Heituao formations were set as 4974–4920 m, 4920–4866 m, 4866–4785 m, 4785–4568 m and 4568–4490 m, respectively. The graptolites zones of *Didymograptus*, *Dicellograptus*, *Phyllograptus*, *Pseudotrigonograptus*, *Climacograptus* and *Orthograptus* found from the 4550–4555 m depth interval (Du et al., 2004), further supported the proposition that the Heituao Formation might be Lower–Middle Ordovician (Fig. 3).

3 Materials and Methods

3.1 Samples

All 216 samples were collected from cuttings of the Tadong2 Well with a depth range of 5000–4500 m and varied sampling intervals, ranging from 2 m to 0.5 m. All samples were washed several times with clean water, then carefully selected to prevent contamination from detached particles and drilling fluid crystals. Each sample was crushed into powder and placed in an aliquot for subsequent analysis.

3.2 Methods

Total organic carbon (TOC), whole-rock $\delta^{13}C_{carb}$ and $\delta^{13}C_{org}$ analyses were carried out in the Key Laboratory of Petroleum Geochemistry, China National Petroleum Corporation. Major element contents of samples within the 5000–4950 m interval were determined in the Beijing Research Institute of Uranium Geology, China National Nuclear Corporation.

Samples for TOC measurement were de-carbonated and combusted in a LECO CS-230HC carbon/sulphur analyzer, following the method described in Zhang et al. (2016). The resulting RSD of each sample was lower than 2.0%.

$\delta^{13}C_{carb}$ and $\delta^{13}C_{org}$ of each sample were determined following the methods described in Canfield et al. (2018). Briefly, pure kerogen was extracted from rocks through HCl and HF treatment as fully described in Zhang et al. (2016). The $\delta^{13}C_{org}$ values were measured on the extracted kerogens by using a Flush EA 1112 HT O/H-N/C combined with a Delta V Advantage mass spectrometer. The mass spectrometer was standardized with GBW04406 ($\delta^{13}C$ =−10.85‰) and GBW04407 ($\delta^{13}C$ = −22.4‰) with RSDs lower than 0.2‰, based on replicate standard analysis. The $\delta^{13}C_{carb}$ of each sample was determined by reaction with phosphoric acid in an online carbonate preparation device and analysis in a Finnigan Mat-252 mass spectrometer (Thermo Scientific). The mass spectrometer was standardized with GBW04405 ($\delta^{13}C$ = 0.57‰, $\delta^{18}O$ = −8.49‰) and GBW04406 ($\delta^{13}C$ = −10.85‰, $\delta^{18}O$ = −12.0‰), with RSDs lower than 0.2‰ based on replicate standard analysis. All $\delta^{13}C$ and $\delta^{18}O$ values were reported relative to the Vienna Pee Dee Belemnite (VPDB), with standard deviation (SD) of each sample being lower than 0.2‰, based on replicate analysis.

Major elements were determined using a Philips PW2400 X-ray fluorescence spectrometer (XRF) and following the methods described in Zhang et al. (2016). The relative standard deviation (RSD) of each element was lower than 1.0%. Accuracies were tested with the shale standard (GBW 03014), that was measured along with the samples. The contents of elements of interest were within 10% of their reported values.

4 Results

4.1 Rough geochemical profiles of the Tadong2 Well within the 5000–4500 m interval

The TOC profile of the 5000–4500 m interval from the Tadong2 Well has a first-order variation of an increase from the upper Ediacaran to the lower Cambrian, then a gradual decrease until the upper Cambrian, followed by another increase to the Lower-Middle Ordovician (Table 1; Fig. 4). Variations of TOC and GR values are basically consistent with the lithological change. Black shales of the Xishanblaq, Xidashan and Heituao formations have high TOC and GR values, while argillaceous limestones of the

Table 1 First-order geochemical profiles of the Tadong2 Well section segmented in formation

Formation	Depth (m)	TOC (%)	$\delta^{13}C_{org}$(‰)	$\delta^{13}C_{carb}$(‰)	$\delta^{18}O_{carb}$(‰)
Heituao	4568–4500	0.35 to 5.06(2.56)	−29.8 to −28.6 (−29.3)	−5.0 to −1.1 (−3.7)	−16.3 to −10.4(−13.5)
Tuershaketage	4785–4568	0.03 to 2.28(1.16)	−27.9 to −24.8 (−26.6)	−0.6 to +3.8 (+1.2)	−10.6 to −7.2 (−8.4)
Mohershan	4866–4785	0.89 to 2.40(1.56)	−28.5 to −26.9 (−27.7)	−2.7 to +0.5 (−1.4)	−9.1 to −6.8 (−8.4)
Xidashan	4919–4866	0.43 to 4.88(2.30)	−30.4 to −28.6 (−29.7)	−5.4 to −1.1 (−2.9)	−12.9 to −6.9 (−9.3)
Xishanblaq	4974–4919	0.08 to 10.0(2.78)	−32.1 to −25.6 (−29.9)	−7.8 to +0.2 (−3.8)	−17.0 to −5.2 (−11.2)
Hankalchough	5000–4974	0.04 to 5.50(1.23)	−30.9 to −24.6 (−29.1)	−5.9 to −0.9 (−2.5)	−12.2 to −4.8 (−7.8)

The maximum and minimum values are outside, while the average values are inside the brackets.

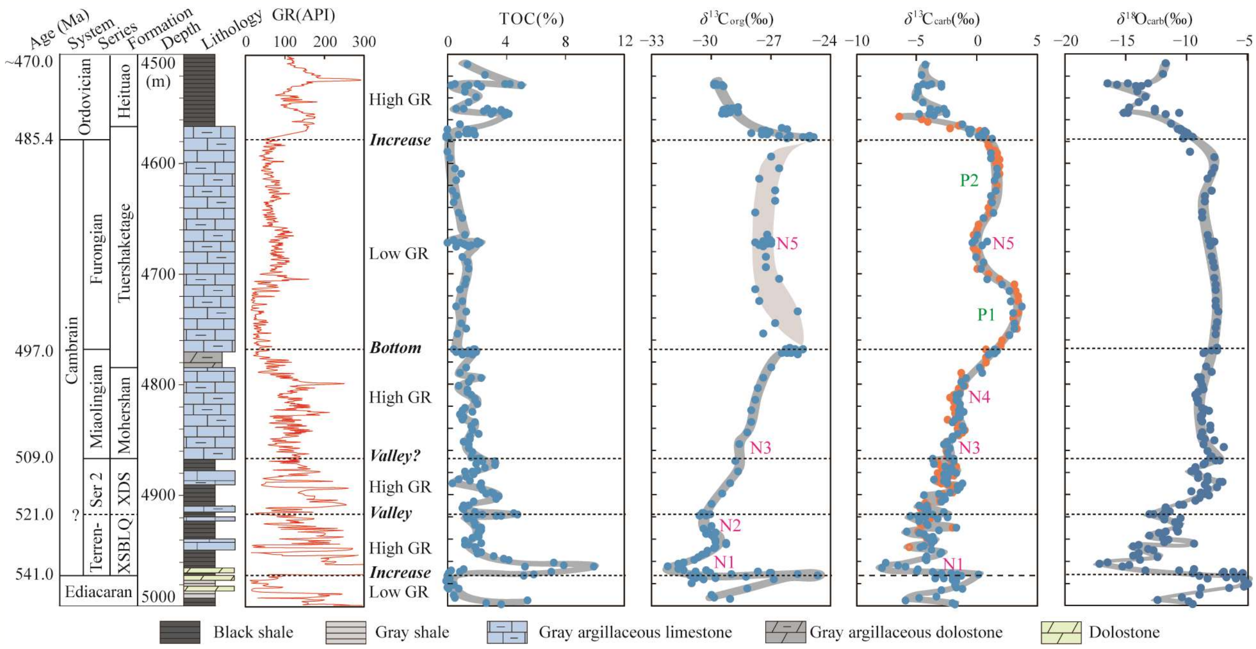

Fig. 4. Geochemical profiles of the Tadong2 Well within the 5000–4500 m interval.

Terren-, Terreneuvian; Ser 2, Series 2; XSBLQ, Xishanblaq; XDS, Xidashan. The question mark and dash line between the Terreneuvian and Series 2 mean the boundary is still uncertain. Shaded curves in TOC, $\delta^{13}C_{org}$, $\delta^{13}C_{carb}$, $\delta^{18}O_{carb}$ panels are suggested geochemical profiles of the Tadong2 Well section. Consistency of referenced $\delta^{13}C_{carb}$ data (orange points) (Chen et al., 2020) and our data (blue points) indicates good reproducibility of the carbon isotope stratigraphy.

Tuershaketage Formation and dolostones of the Hankalchough Formation have low TOC and GR values (Fig. 4). Argillaceous limestones of the Mohershan Formation might have a higher mud content than those of the Tuershaketage Formation, for higher TOC and GR values (Table 1; Fig. 4). It is worth noting that, although TOC values keep oscillating from bottom to top, there are four apogees in the Cambrian TOC profile, at 4965 m, 4918.3 m, 4874 m, 4671.5 m and with a TOC value of 10%, 4.88%, 3.33%, 2.28%, respectively (Fig. 4).

The first-order variations of $\delta^{13}C_{org}$ and TOC profiles are reversed (Table 1; Fig. 4). Compared with frequent TOC fluctuations, there are only two negative excursions in the Cambrian $\delta^{13}C_{org}$ profile. The first one (N1) within the 4974.5–4966 m interval has a nadir of −32.1‰ and a negative excursion of −7.5‰. The second one (N2) within the 4942–4920.5 m interval has a nadir of −30.5‰ and a weak negative excursion of −1.3‰. Upwards from 4920.5 m to 4773.5 m, there is a long-term positive excursion to an apogee of −25.6‰ with a drift value as high as +4.9‰. Argillaceous limestones of the Tuershaketage Formation have low TOC values and fluctuating $\delta^{13}C_{org}$ values (Fig. 4). Overall, $\delta^{13}C_{org}$ values within the 4670–4675 m interval are from −27.7‰ to −27.2‰ (with an average value of −27.2‰), lower than those within the 4768–4773.5 m interval (from −26.4‰ to −25.3‰, with an average value of −25.9‰) and the 4575–4578 m interval (from −26.5‰ to −24.8‰, with an average value of −25.5‰). Upwards from another apogee at the top of the Cambrian, the $\delta^{13}C_{org}$ profile exhibits another large negative excursion (from −24.8‰ to −29.8‰) (Fig. 4).

The first-order variations of $\delta^{13}C_{carb}$ and $\delta^{13}C_{org}$ profiles are the same (Table 1; Fig. 4). However, the $\delta^{13}C_{carb}$ profile has more oscillations in the black shales, including the Xishanblaq and Xidashan formations within the 4974–4875 m interval and the Heituao Formation within the 4565–4500 m interval. On the $\delta^{13}C_{carb}$ profile, N1 displays as the largest negative excursion of about −8‰ (from +0.2‰ to −7.8‰). Frequent oscillations above N1 on the $\delta^{13}C_{carb}$ profile make the declining side of N2 significantly narrower than that on the $\delta^{13}C_{org}$ profile. At the bottom and middle of the Mohershan Formation, two weak negative excursions can be recognized and named N3 (from −1.8‰ at 4867.5 m to −2.7‰ at 4855 m) and N4 (from −1.0‰ at 4825 m to −1.6‰ at 4810 m), respectively. Above 4810 m, there is a large positive excursion (P1) with an apogee of +3.8‰ and a positive drift of +5.4‰. Above P1, there is a negative excursion (N5) of −4.1‰ (from +3.8‰ at 4730 m to −0.3‰ at 4671.5 m,) and another positive excursion (P2) of +2.0‰ (from −0.3‰ at 4671.5 m to +1.7‰ at 4610 m).

Three negative excursions (N1, N2, N5) can be identified on both $\delta^{13}C_{org}$ and $\delta^{13}C_{carb}$ profiles and are accompanied by three apogees on the TOC profile, while another two negative excursions (N3, N4) and two positive excursions (P1, P2) only appear on the $\delta^{13}C_{carb}$ profile and correspond to low TOC values (Fig. 4).

4.2 High-resolution geochemical profiles of the Tadong2 Well within the 5000–4950 m interval

According to lithological features, major element contents (Si, Mg, Ca, P) and TOC values, the 5000–4950 m interval can be further divided into siliceous black shale (4995–5000 m), gray mudstone interlayered with thick dolostone (4995–4978 m), dolostone (4978–4974 m), interbedded black shales and dolostones (4974–4968 m), phosphorus-rich black shale (4968–4966 m) and siliceous black shale (4966–4950 m) (Fig. 5). For the 4974–4968 m interval, the TOC values of black shales are higher than those of interbedded dolostones, while both $\delta^{13}C_{carb}$ and $\delta^{13}C_{org}$ values of black shales are lower (Fig. 5). The maximum values of $\delta^{13}C_{carb}$ and $\delta^{13}C_{org}$ around the Cambrian base appear in dolostones at different depths, while the minimum values of $\delta^{13}C_{carb}$ and $\delta^{13}C_{org}$ appear in black shale with the same depth of 4966 m, just above the phosphorus-rich black shale (Fig. 5).

One negative excursion of both $\delta^{13}C_{carb}$ and $\delta^{13}C_{org}$, named N0, can be identified in the Ediacaran Hankalchough Formation within the 4978–4974 m interval (Fig. 5). It is at the top of the Ediacaran 'cap dolostone' and sits just below N1 around the Cambrian base, with negative excursions of −3.9‰ (from −26.8‰ to −30.7‰) and −1.8‰ (from −1.6‰ to −3.4‰) on $\delta^{13}C_{carb}$ and $\delta^{13}C_{org}$ profiles, respectively. The rising side after N0 has positive excursions of +6.3‰ (from −30.7‰ to −24.6‰) and +3.6‰ (from −3.4‰ to +0.2‰) on $\delta^{13}C_{carb}$ and $\delta^{13}C_{org}$ profiles, respectively.

5 Discussion

5.1 Reliability of carbon isotope values

Diagenetic alteration and fluid interaction may affect

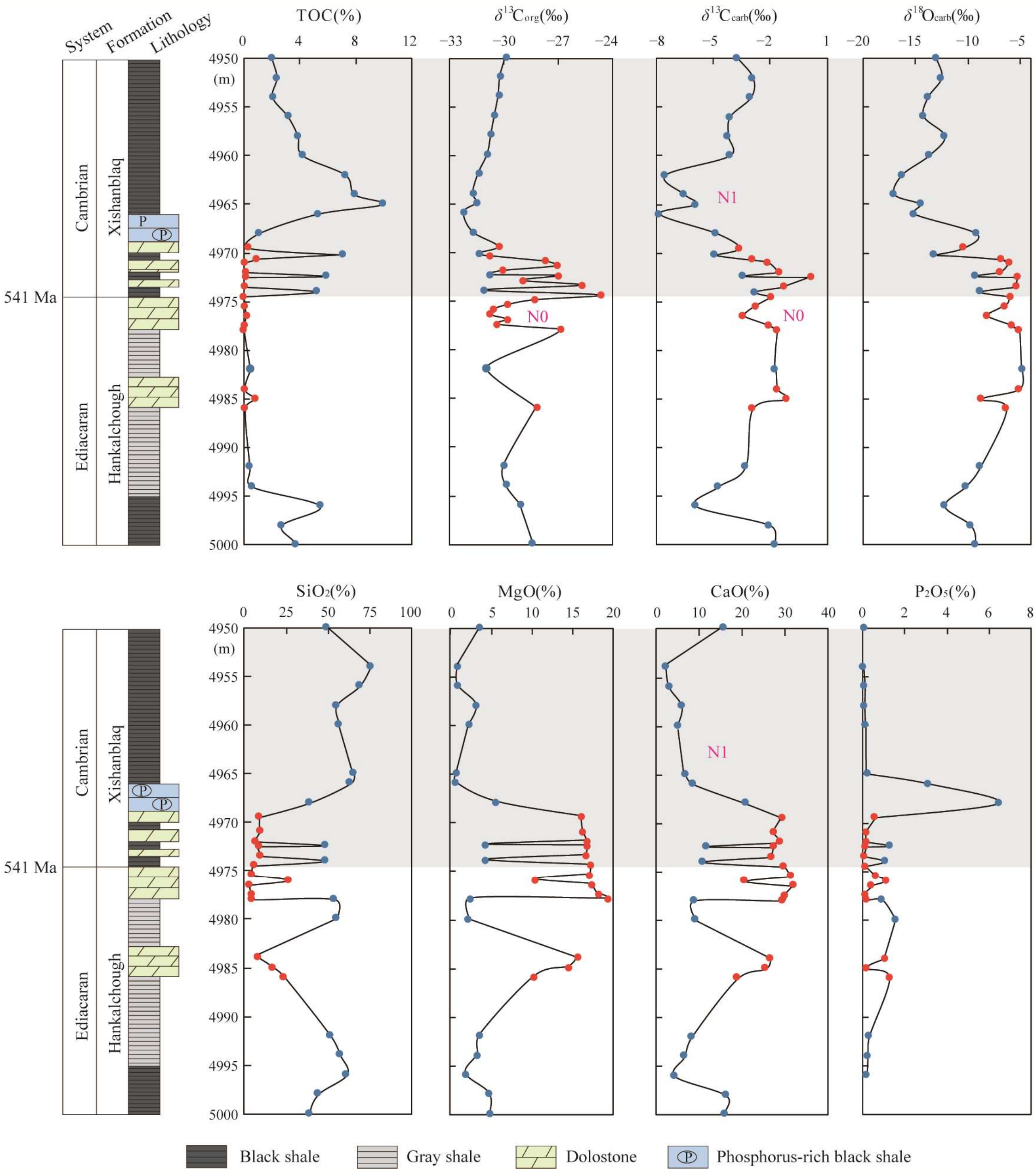

Fig. 5. High-resolution geochemical profiles of the Ediacaran–Cambrian boundary within the 5000–4950 m interval of the Tadong2 Well. Red and blue data are from dolostone and shale, respectively.
Shaded region represents N1 in Fig. 4.

the accuracy and representation of the $\delta^{13}C_{carb}$ value, while the $\delta^{13}C_{org}$ value may be affected by thermal degradation and detrital organic carbon contamination (Marshall, 1992; Jiang et al., 2012). To determine whether $\delta^{13}C_{carb}$ values of ultra-deep rocks represent dissolved inorganic carbon (DIC) information of ancient seawater, it is necessary to exclude possible influences of diagenesis and fluids, which can lead to a significant negative change of $\delta^{18}O_{carb}$ values and/or a positive correlation between $\delta^{13}C_{carb}$ and $\delta^{18}O_{carb}$ values (Marshall, 1992; Schobben et al., 2016). The first-order variation of the $\delta^{18}O_{carb}$ profile is consistent with that of the $\delta^{13}C_{carb}$ profile (Table 1; Fig. 4). However, obvious lithological changes of rocks within the 5000–4500 m interval (Fig. 5) indicate a different sedimentary facies, which might also bring about synergistic variations of $\delta^{13}C_{carb}$ and $\delta^{18}O_{carb}$ values (Marshall, 1992; Drummond et al., 1995). Generally, sediments in deep-water basins have lighter $\delta^{13}C_{org}$, $\delta^{13}C_{carb}$ and $\delta^{18}O_{carb}$ values than those in shallow-water shelfs, such as the sedimentary record of the Ediacaran Doushantuo Formation (Jiang et al., 2011). This is in line with the deep-water deposited black shales of the Xishanblaq, Xidashan and Heituao formations, which have lower $\delta^{13}C_{org}$, $\delta^{13}C_{carb}$ and $\delta^{18}O_{carb}$ values (Table 1; Figs. 4–5). Dividing the rocks in the 5000–4500 m interval into multiple groups according to lithologies reveals no correlation between $\delta^{13}C_{carb}$ and $\delta^{18}O_{carb}$ values in the black shales and carbonate rocks (Fig. 6). Amongst these, no correlation between $\delta^{13}C_{carb}$ and $\delta^{18}O_{carb}$ values was found during positive excursions (P1 and P2, Fig. 6b) and negative excursions (N1 and N2, Fig. 6d–e).

Compared with $\delta^{18}O_{carb}$, diagenesis and fluid interaction have less effect on paired $\delta^{13}C_{carb}$ and $\delta^{13}C_{org}$ values (Marshall, 1992; Maloof et al., 2010). The positive correlation between $\delta^{13}C_{carb}$ and $\delta^{13}C_{org}$ values (R^2 = 0.7017, Fig. 7a) is better than that between $\delta^{13}C_{carb}$ and $\delta^{18}O_{carb}$ values (R^2 = 0.4158, Fig. 7b), indicating conservative and faithful records of the ancient carbon cycle in paired $\delta^{13}C_{carb}$ and $\delta^{13}C_{org}$ values. However, it is still necessary to exclude the possible effects of thermal degradation and detrital organic carbon contamination. During deep burial, $\delta^{13}C_{org}$ values of kerogen may increase by up to +1‰ due to generation of ^{13}C-depleted oil and gas (Clayton, 1991). The present kerogen maturity (R_o) of the lower Cambrian black shales from the Tadong2 Well is about 2.7% (Zhang et al., 2004), higher than the 'oil window' (R_o: 0.7–1.3%), but still in the 'gas window' (R_o: <3.5%) (Pang et al., 2020). As such, the present $\delta^{13}C_{org}$ values should be slightly heavier than those of the primary $\delta^{13}C_{org}$ values. Moreover, thermal degradation and hydrocarbon generation should exist in a similar way throughout the whole section, with a slightly higher maturity in the more deeply buried sediment and organic-rich sediment, due to elevated hydrocarbon generation. For the Tadong2 Well section, the lower Cambrian black shales with higher TOC values and a greater burial depth should have witnessed more heavy isotopic effects on $\delta^{13}C_{org}$ values. Therefore, the lighter $\delta^{13}C_{org}$ values of the lower Cambrian black shales should not result from thermal degradation, but should be inherited from primary buried organic carbon. Detrital organic carbon contamination might exist in pure carbonate sediments with TOC lower than 0.1% (Jiang et al., 2011). However, only 10 of our 216 samples have a TOC value lower than 0.1%, most samples from the Tuershaketage Formation showing heavier $\delta^{13}C_{org}$ values. Such a small amount of data should not affect the original chemostratigraphical trend. At the Ediacaran–Cambrian boundary, organic-poor dolostones and organic-rich black shales show similar isotopic lightening tendencies on both $\delta^{13}C_{carb}$ and $\delta^{13}C_{org}$ profiles (Fig. 5), further confirming the reliability of the obtained carbon isotope values.

5.2 Carbon isotope stratigraphy of the Cambrian System

N1 is just above the Ediacaran–Cambrian boundary and has similar large negative excursions on both $\delta^{13}C_{carb}$ and $\delta^{13}C_{org}$ profiles (Fig. 5). Such large negative excursions of $\delta^{13}C_{carb}$ and $\delta^{13}C_{org}$ also exist in the bottom black shales or dolostones of the Yurtus Formation in the western Tarim Basin, with a nadir $\delta^{13}C_{carb}$ value of −12.4‰ and a nadir $\delta^{13}C_{carb}$ value of −36.5‰ (Yao et al., 2011; Su et al., 2020; Zhang et al., 2020c; Zhang et al., 2022). Not restricted to the Tarim Block, this negative excursion of $\delta^{13}C_{carb}$ at the base of the Cambrian has also been recognized in South China (Ishikawa et al., 2008; Li et al., 2009; Jiang et al., 2012), Siberia (Brasier and Sukhov, 1998; Kouchinsky et al., 2007), Laurentia (Narbonne et al., 1994; Corsetti and Hagadorn, 2000), West Africa (Maloof et al., 2005), Mongolia (Brasier et al., 1996; Smith et al., 2016) and West Asia (Amthor et al., 2003). Therefore, this $\delta^{13}C_{carb}$ negative excursion is considered to be a global carbon cycle perturbation event and is named the BAsal Cambrian Carbon isotope Excursion (BACE) (Zhu et al., 2006) (Fig. 8). As all available biostratigraphic markers appear to be problematic in their ability to accurately constrain the Cambrian base (Zhu et al., 2019) and it is controversial to define the Ediacaran–Cambrian boundary at the onset (Zhu et al., 2006) or nadir (Narbonne et al., 2012) of this negative excursion, the BACE event, with its global indicative significance, is still considered to be the best solution to the problem of defining the base of the Cambrian (Zhu et al., 2019).

According to the suggested Cambrian base at the onset of decreasing $\delta^{13}C$ values from the terminal Ediacaran positive carbon isotope plateau (Zhu et al., 2019), the Ediacaran–Cambrian boundary in the Tadong2 Well becomes one of two possibilities. One is at 4974 m, with the onset of decreasing $\delta^{13}C_{org}$ values, the other is at 4972.5 m, with the onset of decreasing $\delta^{13}C_{carb}$ values (Fig. 5). Since the BACE event is widely considered to be associated with an oxidative reduction of dissolved organic carbon (DOC) reservoir in the context of global transgression and oceanic oxidation (Maloof et al., 2010; Jiang et al., 2012; Ishikawa et al., 2013; Zhang, 2021), ^{13}C -depleted DOC might also have combined with clay minerals and directly entered into sediments, causng a negative excursion of $\delta^{13}C_{org}$ (Zhang, 2021). In contrast, the record in carbonate rocks might be affected by the ancient DIC reservoir size, local sedimentary facies and the blooming of primary productivity, slightly lagging behind the black shale record. Considering the onset of

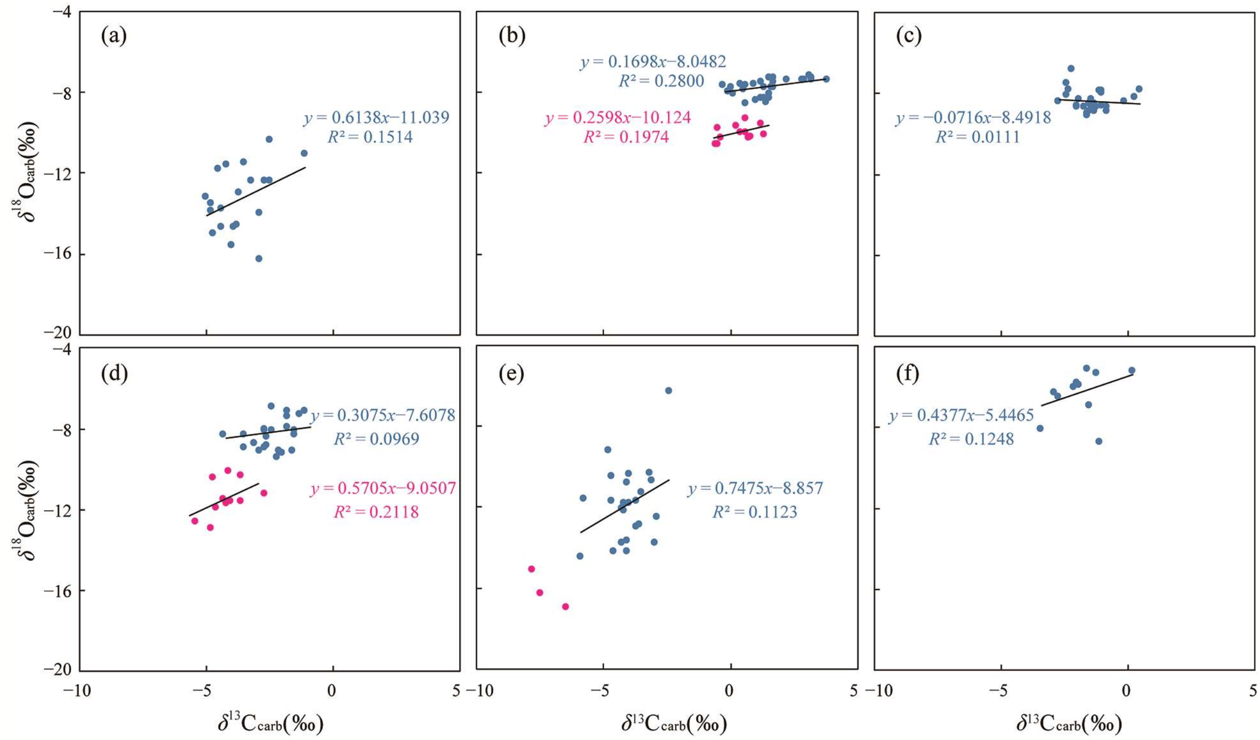

Fig. 6. Correlations of $\delta^{13}C_{carb}$ and $\delta^{18}O_{carb}$ values segmented in formation.
(a) Heituao Formation; (b) Tuershaketage Formation (pink and blue data are samples of P1 and P2, respectively); (c) Mohershan Formation; (d) Xidashan Formation (pink and blue data are samples of N2 and the rest, respectively); (e) Xishanblaq Formation (pink and blue data are 3 samples from the peak of N1 and the rest, respectively); (f) dolostones from the Hankalchough and Xishanblaq formations.

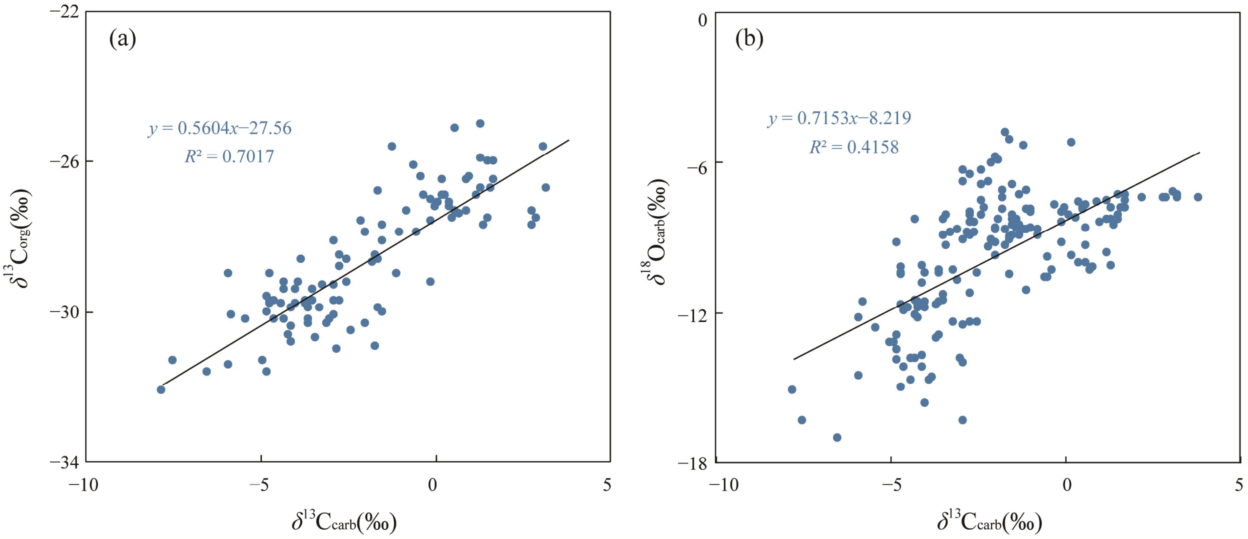

Fig. 7. Correlations of (a) $\delta^{13}C_{carb}$ and $\delta^{13}C_{org}$ values and (b) $\delta^{13}C_{carb}$ and $\delta^{18}O_{carb}$ values.

decreasing $\delta^{13}C_{org}$ values of 4974 m is at the appearance of the black shale and the base of the Xiaoerbulake Formation (Fig. 5), this is proposed to represent the base of the Cambrian in the Tadong2 Well. This depth also corresponds to a sharp increase in the GR profile (Fig. 4).

Above N1, $\delta^{13}C_{carb}$ values oscillate up until the nadir of N3 at the base of the Mohershan Formation. However, the $\delta^{13}C_{org}$ profile has only one negative excursion (N2), with a nadir at 4919 m, the base of the Xidashan Formation (Fig. 4). The GR profile also displays a valley around this depth for high GR values of the Xishanblaq and Xidashan rocks (Fig. 4). Assuming that the Xidashan Formation is isochronous with Series 2 (Zhang, 1983; Zhu and Lin, 1983), 4919 m in the Tadong2 Well was proposed as representing the base of Series 2, corresponding with a nadir or a valley on $\delta^{13}C_{org}$ and GR profiles, as well as one of the apogees on the TOC profile (Fig. 4).

The FAD of *Oryctocephalus indicus* coincided with the extinction of olenellid and redlichiid trilobites (Zhao et al., 2014) and the ROECE event (Zhu et al., 2004a).

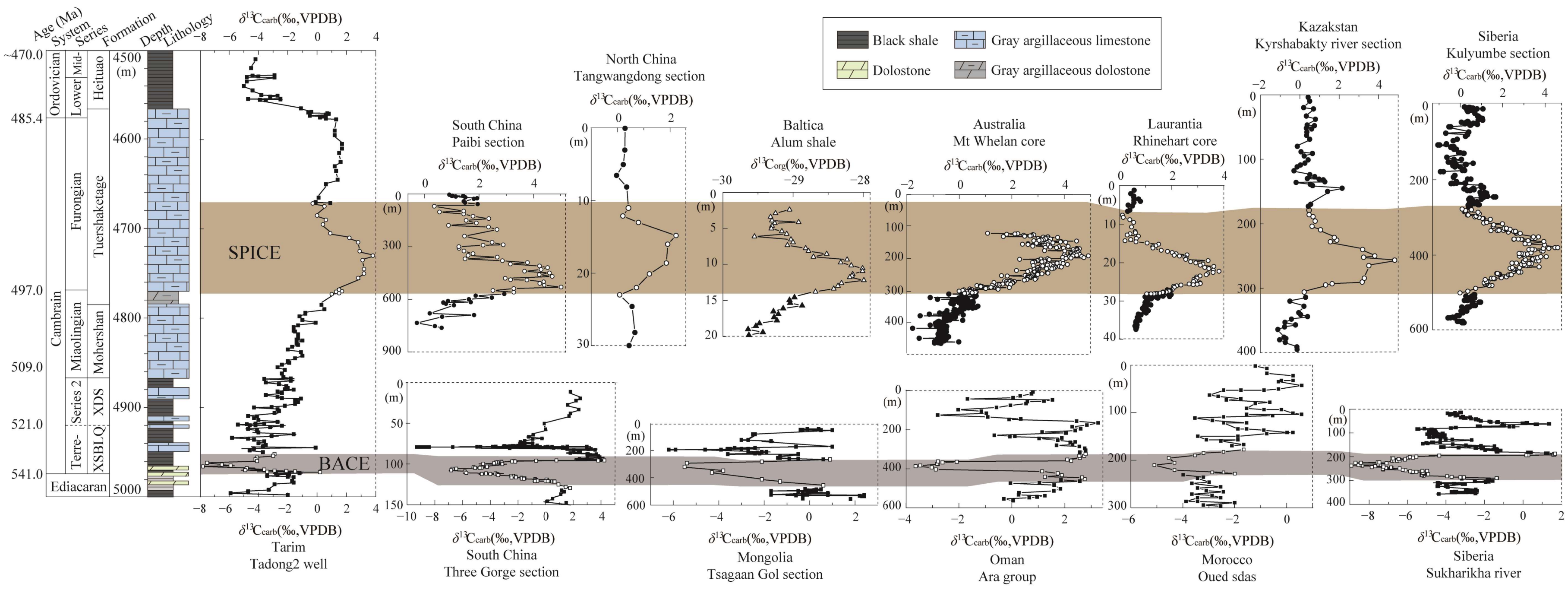

Fig. 8. Global correlation of the Cambrian carbon isotope stratigraphy of the Tadong2 Well section from the eastern Tarim Basin.

Data sources, Three Gorge section in South China (Ishikawa et al., 2008); Sukharikha river section in Siberia (Brasier and Sukhov, 1998); Oued sdas section in Morocco (Maloof et al., 2005); Tsagaan Gol section in Mongolia (Brasier et al., 1996); Ara Group in Oman (Amthor et al., 2003); Tangwangdong section in North China (Ripperdan et al., 1993), Paibi section in South China (Peng et al., 2004), Kyrshabakty River section in Kazakhstan (Saltzman et al., 2000), Kulyumbe section in Siberia (Kouchinsky et al., 2008), Mt. Whelan core in Australia (Saltzman et al., 2000), Rhinehart core in Laurentia (Saltzman et al., 1998), Alum Shale Formation in Baltica (Ahlberg et al., 2009). Open circles are isotopic records during the BACE and SPICE events.

Oryctocephalus indicus has been found at the bottom of the Mohershan Formation (or the Chuanxingshan Formation mentioned in Zhang, 1990), thus N3 might be the ROECE around the Miaolingian base (Fig. 4). This negative excursion has been found in the Keping section in the western Tarim Basin (Wang et al., 2011; Guo et al., 2017; Zhang et al., 2020c) and other blocks, such as South China (Zhu et al., 2004a; Zuo et al., 2018), North China (Zhu et al., 2004a), Australia (Schmid, 2017), Laurentia (Montañez et al., 2000), western America (Luke et al., 2017), northwestern Scotland (Faggetter et al., 2018) and southern Britain (Harvey et al., 2011). Similar to the BACE event, it is still difficult to define the Miaolingian base at the onset or nadir of ROECE. In the Tadong2 Well, 4866 m is the base of the Mohershan Formation and is accompanied by the onset of decreasing $\delta^{13}C_{carb}$ values, the disappearance of black shale and an indistinct valley on the GR profile (Fig. 4). Therefore, 4866 m in the Tadong2 Well is suggested to be the Miaolingian base.

N4 is a weak negative excursion in the middle of the Mohershan Formation (Fig. 4), where *Ptychagnostus atavus* has been found (Zhang, 1990) and coincides with the DICE event at the base of the Drumian Stage (Zhu et al., 2019). Thus, N4 might be the DICE, which has been found in the west and middle of the Tarim Basin (Chen et al., 2019; Yang et al., 2021) and other blocks, such as South China (Li et al., 2020), North China (Zhu et al., 2004b), Siberia (Brasier and Sukhov, 1998), Baltica (Ahlberg et al., 2009; Álvaro et al., 2008), Australia (Schmid, 2017), Laurentia (Montañez et al., 2000) and western America (Howley and Jiang, 2010). Differing in its high GR and TOC values and large $\delta^{13}C_{org}$ negative excursion of the sediments during the BACE event, sediments during the DICE event correspond tolow GR and TOC values without variation in the $\delta^{13}C_{org}$ positive excursion trend (Fig. 4). This might be related to the end of the oxidation process of the DOC reservoir and the stabilization of the carbon cycle and climate change.

On the $\delta^{13}C_{carb}$ profile, P1 is a long-term positive excursion until an apogee at 4730 m with a $\delta^{13}C_{carb}$ value of +3.8‰. Combined with the boundary of *Glyptagnostus reticulatus* and *Glyptagnostus stolidotus* (R/S) at the bottom of the Tuershaketage Formation (Zhang, 1990), P1 should be the unambiguous and widely-documented SPICE (Fig. 8). The SPICE event has already been found in the Tarim Basin (Liu et al., 2017; Chen et al., 2020) and many other blocks, such as North China (Ripperdan et al., 1993), South China (Peng et al., 2004; Zhu et al., 2004b), Kazakhstan (Saltzman et al., 2000), Avalonia (Woods et al., 2011), Siberia (Kouchinsky et al., 2008), Australia (Saltzman et al., 2000; Schmid, 2017), Laurentia (Saltzman et al., 1998; Saltzman et al., 2004), Baltica (Álvaro et al., 2008; Ahlberg et al., 2009), South America (Sial et al., 2013) and northern Scotland (Pruss et al., 2019). Detailed study of the isotopic curves showed that both the onset and apogee of SPICE were anachronous and varied in different blocks. In South China, Australia and Baltica, the R/S boundary is in the middle of the rising side. However, in Laurentia, Siberia and Kazakhstan, it is associated with the onset of the rise. In the Tadong2 Well section, the onset of the rising side is the nadir of DICE, which clearly cannot be used as the Furongian base. Fossil evidence is absent from the Tadong2 Well. Fortunately, the $\delta^{13}C_{org}$ profile has two obvious apogees at the bottom and top of the Tuershaketage Formation. Referring to the practice of BACE, 4770 m with an apogee $\delta^{13}C_{org}$ value was suggested as the Furongian base (Fig. 4).

Similar to the Ediacaran-Cambrian boundary, the Cambrian–Ordovician boundary also shows a sharp increase in GR profile with an apogee of 4578 m on the $\delta^{13}C_{org}$ profile (Fig. 4). Overall, the Furongian sediments have lower GR values than other Cambrian and Ordovician sediments, exhibiting the minimum value around 4770 m to 4578 m (Fig. 4). This feature makes the base and apex of the Furongian quite identifiable on the GR profile, with two boundary depths highly consistent with apogees on the $\delta^{13}C_{org}$ profile (Fig. 4). Both the base and the apex of the Furongian are in the Tuershaketage Formation, being similar with their positions in outcrop sections based on biostratigraphy (Zhang, 1990; Lin et al., 2001). However, on the $\delta^{13}C_{carb}$ profile, these two boundaries locate exactly in the middle of the rising side of P1 and the declining side of P2, respectively (Fig. 4). Thus, if only referring to the $\delta^{13}C_{carb}$ profile, it is difficult to determine their exact positions.

Based on the above discussion, the suggested base depths of the Terreneuvian, Series 2, Miaolingian and Furongian and Lower Ordovician in the Tadong2 Well are 4974 m, 4919 m, 4866 m, 4770 m and 4578 m, respectively, which correspond to valley or bottom values on the GR profile. In addition, we roughly calculated the deposition rates during the Terreneuvian, Series 2, Miaolingian, Furongian to be 0.28, 0.44, 0.80 and 1.65 cm per thousand years (cm/kyr), respectively.

5.3 Implications for the Cambrian source rock distribution and ultra-deep oil and gas exploration in the Tarim Basin

Paired analysis of $\delta^{13}C_{carb}$ and $\delta^{13}C_{org}$ could avoid inaccuracy from interference for carbonate or shale dominated sequences and provide an indicator to interpret the global carbon cycle and transformation between oceanic DIC and DOC (Jiang et al., 2012; Li et al., 2020; Zhang et al., 2020b). Large and synchronized excursions of $\delta^{13}C_{carb}$ and $\delta^{13}C_{org}$ indicate great perturbations of the global carbon cycle. Multiple large negative excursions of $\delta^{13}C_{carb}$ (such as WANCE, Shuram, BACE, DICE) during the Ediacaran and Cambrian periods have been considered to be related to oxidations of oceanic DOC reservoirs after the Neoproterozoic Oxygenation Event (NOE) (Rothman et al., 2003; Ishikawa et al., 2013; Li et al., 2020; Chen et al., 2022). The BACE event, with the largest and widespread negative $\delta^{13}C_{carb}$ excursion, should be a huge and high-intensity oxidant input into the ocean at the beginning of the Phanerozoic Era. The Cambrian oxidant entering the ocean might not only be high-latitude oxygen-rich cold water, but also contain sulfate through terrestrial oxic weathering (Li et al., 2020). The former might reach continental marginal basins along with ocean circulation and upwelling and cause the deep ocean to be oxidized, while the latter might consume organic matter in the water column through sulfate reduction reactions and generate

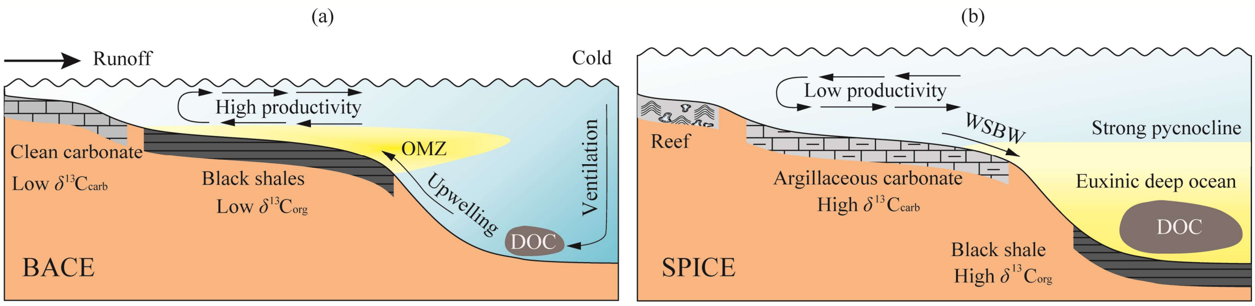

Fig. 9. Inferred paleo-ocean environment during the BACE (a) and SPICE (b) events.
OMZ, oxygen minimum zone; WSBW, warm saline bottom water.

large amounts of H_2S (Zhang et al., 2016). Therefore, the early Cambrian ocean during the BACE event might develop oxygen minimum zones (OMZs), widespread along continental margins (Fig. 9a), which have already been confirmed in the Baltic and South China blocks (Guilbaud et al., 2018; Ye et al., 2022). The bio-toxic H_2S in the water column over shelf and slope might have contributed to the extinction of small shelled organisms and Ediacaran organisms, forming a long-term fossil-depleted belt during 541–521 Ma (Zhu et al., 2019). However, the OMZ environment is conducive to the blooming of nitrogen-fixing micro-organisms (such as cyanobacteria and sulfur bacteria) and the preservation of organic carbon (Ulloa et al., 2012; Scholz, 2018), thus forming the lower Cambrian black shales.

The lower Cambrian black shale in the Tarim Basin corresponds to a significant DOC reservoir oxidation event, demonstrating that deep-time Earth system evolution is of great significance to the formation of oil and gas resources. The presence of an euxinic environment on slope facies during the lower Cambrian black shale deposition in the Tarim Basin has been widely confirmed by high contents of biomarkers of green sulfur bacteria and heavy sulfur isotopes of pyrite ($\delta^{34}S_{py}$) (Cai et al., 2009; Zhang et al., 2020a; He et al., 2022), a negative excursion in bulk rock isotopes of nitrogen ($\delta^{15}N$) (Su et al., 2020) and proxies of redox-sensitive elements (such as Mo, V, and U) (Zhu et al., 2021a; Zhu et al., 2021b; He et al., 2022). Although Zhu et al. (2021a) has noted some intermittent oxidation features during the deposition of the Yurtus black shales in the western Tarim Basin, direct evidence of oxidized bottom water has not been found in the eastern Tarim Basin. According to large negative excursions of both $\delta^{13}C_{carb}$ and $\delta^{13}C_{org}$ in the Tarim Basin (Fig. 10a), it can still be speculated that a large-scale DOC reservoir oxidation event might have occurred. Since the hydrocarbon generating potential of sedimentary organic matter in a weakly oxidized environment is lower than in an euxinic environment (Wang et al., 2021), the hydrocarbon contribution of the lower Cambrian black shales in the Tarim Basin might mainly come from the sediments in the slope, rather than in the deep basin.

The SPICE event lasted for about five trilobite zones, with an estimated duration of 2–4 million years (Myr), much longer than the mean residence time of oceanic carbon (~350 kyr) (Saltzman et al., 1998), indicating another interrupted steady-state of oceanic DIC. The SPICE event has been interpreted to be associated with widespread oceanic anoxia and a massive burial of organic carbon (Saltzman et al., 1998; Saltzman et al., 2004; Álvaro et al., 2008; Gill et al., 2011; Saltzman et al., 2011). However, in the Tadong2 Well located in the eastern Tarim Basin, sediments during the SPICE event are mainly argillaceous limestones with low TOC values (Fig. 4; Table 1). A similar situation exists in Laurentia, South China, North China and Australia and other blocks with massive carbonate deposition (Saltzman et al., 2011; Woods et al., 2011). The Alum Formation in Baltica is the only exception, with thick and organic-rich black shale (Ahlberg et al., 2009; Hammer and Svensen, 2017). Therefore, there is still no evidence for widespread black shales coinciding with the positive excursion of the SPICE event. Although black shales might be restricted to deep basins rather than shelf or shelf margins that were inferred to be the depositional setting in most studies (Álvaro et al., 2008; Woods et al., 2011), another possible explanation is that organic carbon might not enter into sediments, but rather be fixed in the form of DOC, causing an expansion of the DOC reservoir during the SPICE oceanic anoxic event (Fig. 9b).

In the Tarim Basin, sediments during the SPICE event were dominated by limestone or argillaceous limestone that was deposited on the platform or on platform margins. Positive excursions of $\delta^{13}C_{carb}$ in the eastern Tarim Basin (Tadong2 Well and Yaerdang Mountain outcrop section) are higher than those in the west and middle of the Tarim Basin (Shutan1, Yingtan1 and Zhongshen1 wells) (Fig. 10b), indicating that more organic carbon might be buried or fixed in the East Depression and cause obvious carbon isotope fractionation of the ancient DIC reservoir. The expanded DOC reservoir during the Furongian Series might have been oxidized again in the Early Ordovician and cause another synchronized negative excursion of both $\delta^{13}C_{carb}$ and $\delta^{13}C_{org}$ accompanying black shale deposition (Fig. 4). Therefore, the formation of the Heituao black shale could arguably be viewed as having been 'rooted' in the SPICE, for the storage of organic carbon in the form of DOC in the deep ocean. Even so, the Furongian sediments in the Tadong2 Well have an average TOC value over 1%, with a relatively high deposition rate (1.65 cm/kyr). With the assumption of rock density of 2.2 kg/m^3, a roughly calculated average organic carbon burial rate during the Furongian period can reach 0.42 kg/m^2 kyr, much higher than that of the Terreneuvian, Series 2 and

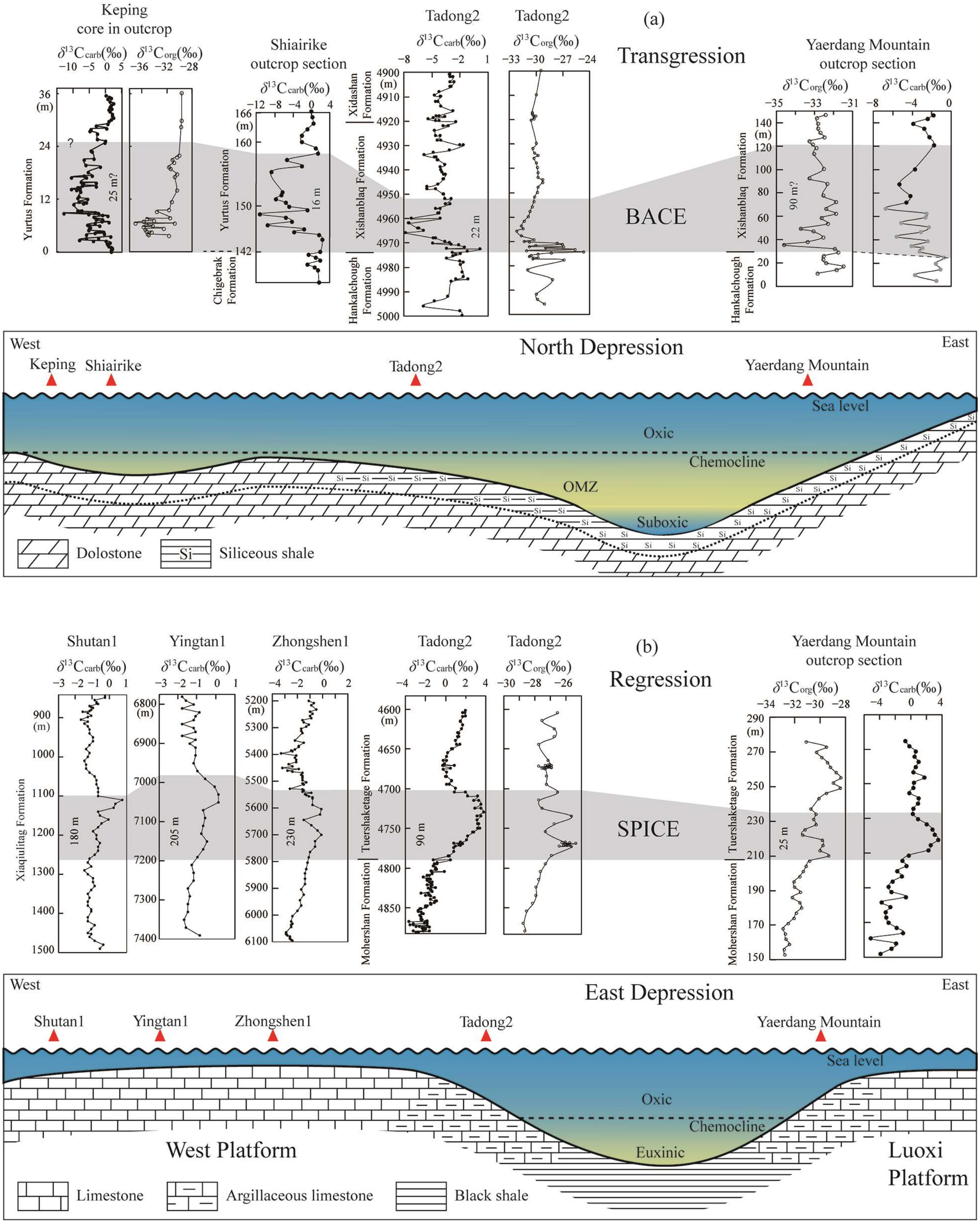

Fig. 10. The BACE (a) and SPICE (b) records in the Tarim Basin and inferred paleo-oceanic environment.

Data source, Keping (Su et al., 2020); Shiairike (Deng et al., 2021); Yaerdang Mountain (Liu et al., 2017); Shutan1, Yingtan1 and Zhongshen1 wells (Chen et al., 2020).

Miaolingian of 0.22, 0.23 and 0.27 kg/m^2 kyr, respectively. This indicates that more organic carbon was fixed in the Furongian sediments than in other Cambrian sediments. Therefore, we can still predict the existence of organic-rich black shales in the deep-water and anoxic depositional environments of the East Depression (Fig.

10b).

6 Conclusions

The sequence preserved in the eastern Tarim Basin represents a complete Cambrian sedimentary record with a better stratigraphic continuity than in the western Keping region. According to the integrated $\delta^{13}C_{carb}$ and $\delta^{13}C_{org}$ profiles of the Tadong2 Well, BACE, ROECE, DICE and SPICE were recognized and used to determine the base of each series of the Cambrian System. New proposed Cambrian carbon isotope stratigraphy is easy to identify and consistent with previous biostratigraphy in the outcrop sections. For the abnormal carbon isotope anomalies and organic carbon burials in the Tarim Basin, especially during the BACE and SPICE events, a huge DOC reservoir is suggested to have existed in the East Depression that experienced a reduction and expansion cycle. Based on these, the ultra-deep petroleum exploration in the Tarim Basin was proposed to be implemented according to the different paleogeographic and carbon cycle characteristics during each series of the Cambrian Period. The lower Cambrian black shale with high TOC values in slope facies should be the focus of attention. The upper Cambrian black shale might be deposited in the deep water of the East Depression and contribute to hydrocarbon generation. This is a new field worthy of attention. Therefore, this study provides new insights for the division of the Cambrian System, based on carbon isotope stratigraphy and the correlation of deep-time Earth system evolution with ultra-deep petroleum exploration.

Acknowledgments

This research was financially supported by the National Key Research and Development Program of China (2017YFC0603101), the Strategic Priority Research Program of the Chinese Academy of Sciences (XDA14010101) and the National Natural Science Foundation of China (41872125, 42102146, 42002158).

Manuscript received Feb. 14, 2022
accepted Apr. 15, 2022
associate EIC: ZHANG Shuichang
edited by Jeffery J. LISTON and FEI Hongcai

References

Ahlberg, P., Axheimer, N., Babcock, L.E., Eriksson, M.E., Schmitz, B., and Terfelt, F., 2009. Cambrian high-resolution biostratigraphy and carbon isotope chemostratigraphy in Scania, Sweden: First record of the SPICE and DICE excursions in Scandinavia. Lethaia, 42(1): 2–16.

Alcott, L.J., Mills, B.J., and Poulton, S.W., 2019. Stepwise Earth oxygenation is an inherent property of global biogeochemical cycling. Science, 366(6471): 1333–1337.

Álvaro, J.J., Bauluz, B., Subías, I., Pierre, C., and Daniel, V., 2008. Carbon chemostratigraphy of the Cambrian–Ordovician transition in a midlatitude mixed platform, Montagne Noire, France. Geological Society of America Bulletin, 120(7–8): 962–975.

Amthor, J.E., Grotzinger, J.P., Schröder, S., Bowring, S.A., Ramezani, J., Martin, M.W., and Matter, A., 2003. Extinction of Cloudina and Namacalathus at the Precambrian–Cambrian boundary in Oman. Geology, 31(5): 431–434.

An, D.S., and Zhang, Q.T., 1986. The Cambrian and Ordovician strata in the Querqueke and Yaerdangshan Mountains, Xinjiang. Regional Geology of China, (2): 115–124 (in Chinese with English abstract).

Bai, Z.K., Cheng, M.H., Chen, C., Huo, J.Z., Zhang, J.F., Zhou, X.G., Gao, Y.J., Zhao, B., Qiu, H.J., and Han, M., 2020. Distribution features of the Nanhua-Sinian rifts and their significance to hydrocarbon accumulation in the Tarim Basin. Acta Geologica Sinica (English Edition), 94(2): 501–515.

Brasier, M.D., Shields, G., Kuleshov, V.N., and Zhegallo, E.A., 1996. Integrated chemo- and biostratigraphic calibration of early animal evolution: Neoproterozoic–early Cambrian of southwest Mongolia. Geological Magazine, 133(4): 445–485.

Brasier, M.D., and Sukhov, S.S., 1998. The falling amplitude of carbon isotopic oscillations through the Lower to Middle Cambrian: Northern Siberia data. Canadian Journal of Earth Sciences, 35(4): 353–373.

Cai, C.F., Li, K.K., Anlai, M., Zhang, C.M., Xu, Z.M., Worden, R.H., Wu, G.H., Zhang, B.S., and Chen, L.X., 2009. Distinguishing Cambrian from Upper Ordovician source rocks: Evidence from sulfur isotopes and biomarkers in the Tarim Basin. Organic Geochemistry, 40(7): 755–768.

Cai, X.Y., Dou, L.W., Jiang, H.S., Yu, T.X., and Cao, Z.C., 2014. Classification and correlation of cambrian in eastern Tarim basin. Petroleum Geology & Experiment, 36(5): 539–545 (in Chinese with English abstract).

Canfield, D.E., Zhang, S.C., Wang, H.J., Wang, X.M., Zhao, W.Z., Su, J., Bjerrum, C., Haxen, E., and Hammarlund, E., 2018. A Mesoproterozoic Iron Formation. Proceedings of the National Academy of Sciences of the United States of America, 115(17): E3895–E3904.

Chen, B., Hu, C.L., Mills, B.J., He, T.C., Andersen, M.B., Chen, X., Liu, P.J., Lu, M., Newton, R.J., and Poulton, S.W., 2022. A short-lived oxidation event during the early Ediacaran and delayed oxygenation of the Proterozoic ocean. Earth and Planetary Science Letters, 577: 117274.

Chen, X., BergstrÖm, S.M., Zhang, Y.D., and Fan, J.X., 2009. The base of the Middle Ordovician in China with special reference to the succession at Hengtang near Jiangshan, Zhejiang Province, southern China. Lethaia, 42: 218–230.

Chen, Y.Q., Zhang, Y.Q., Wu, Y.S., Zhou, P., Li, K.K., and Wang, X.X., 2020. Discovery of SPICE and carbon isotope stratigraphic correlation of the Cambrian Furongian Series in Tarim Craton, NW China. Science China Earth Sciences, 63 (9): 1330–1338.

Chen, Y.Q., Zhang, Y.Q., Zhou, P., and Alimu, K., 2019. Carbon isotope stratigraphy and correlation of the Cambrian Miaolingian strata, Tarim Basin. Journal of Stratigraphy, 43 (3): 324–332.

Clayton, C.J., 1991. Effect of maturity on carbon isotope ratios of oils and condensates. Organic Geochemistry, 17(6): 887–899.

Cooper, R.A., Nowlan, G.S., and Williams, S.H., 2001. Global Stratotype Section and Point for base of the Ordovician System. Episodes, 24(1): 19–28.

Corsetti, F.A., and Hagadorn, J.W., 2000. Precambrian–Cambrian transition: Death Valley, United States. Geology, 28 (4): 299–302.

Deng, Q., Wang, H.Z., Wei, Z.W., Li, S.D., Zhang, H.Z., Liu, H., Faboya, O.L., Cheng, B., and Liao, Z.W., 2021. Different accumulation mechanisms of organic matter in Cambrian sedimentary successions in the western and northeastern margins of the Tarim Basin, NW China. Journal of Asian Earth Sciences, 207: 104660.

Dong, L., Xiao, S.H., Shen, B., Zhou, C.M., Li, G.X., and Yao, J.X., 2009. Basal Cambrian microfossils from the Yangtze Gorges area (South China) and the Aksu area (Tarim block, northwestern China). Journal of Paleontology, 83(1): 30–44.

Drummond, C.N., Patterson, W.P., and Walker, J.C., 1995. Climatic forcing of carbon–oxygen isotopic covariance in temperate–region marl lakes. Geology, 23(11): 1031–1034.

Du, P.D., Zhan, S.G., Huang, Z.B., Li, M., and Zhao, Z.X., 2004. The Ordovacian Graptolites from the Tadong–2 borehole of the Tarim Basin. Journal of Stratigraphy, 28(1): 56–58 (in

Chinese with English abstract).
Faggetter, L.E., Wignall, P.B., Pruss, S.B., Sun, Y.D., Raine, R.J., Newton, R.J., Widdowson, M., Joachimski, M.M., and Smith, P.M., 2018. Sequence stratigraphy, chemostratigraphy and facies analysis of Cambrian Series 2–Series 3 boundary strata in northwestern Scotland. Geological Magazine, 155(4): 865–877.
Fu, D.J., Tong, G.H., Dai, T., Liu, W., Yang, Y.N., Zhang, Y., Cui, L.H., Li, L.Y., Yun, H., and Wu, Y., 2019. The Qingjiang biota—A Burgess Shale–type fossil Lagerstätte from the early Cambrian of South China. Science, 363(6433): 1338–1342.
Gill, B.C., Lyons, T.W., Young, S.A., Kump, L.R., Knoll, A.H., and Saltzman, M.R., 2011. Geochemical evidence for widespread euxinia in the Later Cambrian Ocean. Nature, 469 (7328): 80–83.
Guan, S.W., Zhang, C.Y., Ren, R., Zhang, S.C., Wu, L., Wang, L., Ma, P.L., and Han, C.W., 2019. Early Cambrian syndepositional structure of the northern Tarim Basin and a discussion of Cambrian subsalt and deep exploration. Petroleum Exploration and Development, 46(6): 1141–1152.
Guilbaud, R., Slater, B.J., Poulton, S.W., Harvey, T.H., Brocks, J.J., Nettersheim, B.J., and Butterfield, N.J., 2018. Oxygen minimum zones in the early Cambrian ocean. Geochemical Perspectives Letters, 6: 33–38.
Guo, Q.J., Deng, Y.N., Hu, J., and Wang, L.Y., 2017. Carbonate carbon isotope evolution of seawater across the Ediacaran–Cambrian transition: Evidence from the Keping area, Tarim Basin, NW China. Geological Magazine, 154(6): 1244–1256.
Hammer, Ø., and Svensen, H.H., 2017. Biostratigraphy and carbon and nitrogen geochemistry of the SPICE event in Cambrian low–grade metamorphic black shale, Southern Norway. Palaeogeography, Palaeoclimatology, Palaeoecology, 468: 216–227.
Harvey, T.H., Williams, M., Condon, D.J., Wilby, P.R., Siveter, D.J., Rushton, A.W., Leng, M.J., and Gabbott, S.E., 2011. A refined chronology for the Cambrian succession of southern Britain. Journal of the Geological Society, 168(3): 705–716.
Hayes, J.M., Strauss, H., and Kaufman, A.J., 1999. The abundance of ^{13}C in marine organic matter and isotopic fractionation in the global biogeochemical cycle of carbon during the past 800 Ma. Chemical Geology, 161(1): 103–125.
He, T.H., Li, W.H., Lu, S.F., Pan, W.Q., Ying, J.F., Zhu, P.F., Yang, E.,Q. Wang, X.Z., Zhang, B.S., and Sun, D.Q., 2022. Mechanism and geological significance of anomalous negative $\delta^{13}C_{kerogen}$ in the Lower Cambrian, NW Tarim Basin, China. Journal of Petroleum Science and Engineering, 208: 109384.
Howley, R.A., and Jiang, G.Q., 2010. The Cambrian Drumian carbon isotope excursion (DICE) in the Great Basin, western United States. Palaeogeography Palaeoclimatology Palaeoecology, 296(1–2): 138–150.
Huang, Z.B., Liu, L.J., Yang, H.J., Wu, Y.S., Yang, Z.L., Zhao, R., Xiao, Z.Y., and Pan, W.Q., 2017. The spatial-temporal distribution of paleocommunities on the Cambrian platform of the Tarim block and its stratigraphic significances. Journal of Stratigraphy, 41(1): 1–16 (in Chinese with English abstract).
Ishikawa, T., Ueno, Y., Komiya, T., Sawaki, Y., Han, J., Shu, D.G., Li, Y., Maruyama, S., and Yoshida, N., 2008. Carbon isotope chemostratigraphy of a Precambrian/Cambrian boundary section in the Three Gorge area, South China: Prominent global–scale isotope excursions just before the Cambrian Explosion. Gondwana Research, 14(1–2): 193–208.
Ishikawa, T., Ueno, Y., Shu, D.G., Li, Y., Han, J., Guo, J.F., Yoshida, N., and Komiya, T., 2013. Irreversible change of the oceanic carbon cycle in the earliest Cambrian: High-resolution organic and inorganic carbon chemostratigraphy in the Three Gorges area, South China. Precambrian Research, 225: 190–208.
Jenkyns, H.C., 2010. Geochemistry of oceanic anoxic events. Geochemistry, Geophysics, Geosystems, 11(3): 1–30.
Jiang, G.Q., Shi, X.Y., Zhang, S.H., Wang, Y., and Xiao, S.H., 2011. Stratigraphy and paleogeography of the Ediacaran Doushantuo Formation (ca. 635–551 Ma) in South China. Gondwana Research, 19(4): 831–849.
Jiang, G.Q., Wang, X.Q., Shi, X.Y., Xiao, S.H., Zhang, S.H., and Dong, J., 2012. The origin of decoupled carbonate and organic carbon isotope signatures in the early Cambrian (ca. 542–520 Ma) Yangtze platform. Earth and Planetary Science Letters, 317: 96–110.
Kouchinsky, A., Bengtson, S., Gallet, Y., Korovnikov, I., Pavlov, V., Runnegar, B., Shields, G.A., Veizer, J., Young, E., and Ziegler, K., 2008. The SPICE carbon isotope excursion in Siberia: A combined study of the upper Middle Cambrian–lowermost Ordovician Kulyumbe River section, northwestern Siberian Platform. Geological Magazine, 145(5): 609–622.
Kouchinsky, A., Bengtson, S., Pavlov, V., Runnegar, B., Torssander, P., Young, E., and Ziegler, K., 2007. Carbon isotope stratigraphy of the Precambrian–Cambrian Sukharikha River section, northwestern Siberian platform. Geological Magazine, 144(4): 609–618.
Kump, L.R., and Arthur, M.A., 1999. Interpreting carbon isotope excursions: Carbonates and organic matter. Chemical Geology, 161(1): 181–198.
Li, D., Ling, H.F., Jiang, S.Y., Pan, J.Y., Chen, Y.Q., Cai, Y.F., and Feng, H.Z., 2009. New carbon isotope stratigraphy of the Ediacaran–Cambrian boundary interval from SW China: Implications for global correlation. Geological Magazine, 146 (04): 465–484.
Li, D.D., Zhang, X.L., Zhang, X., Zhu, H., Peng, S.C., Sun, L.L., and Shen, Y.N., 2020. A paired carbonate–organic δ^{13}C approach to understanding the Cambrian Drumian carbon isotope excursion (DICE). Precambrian Research, 349: 105503.
Lin, T.R., Zhang, T.R., Lin, H.L., and Zhou, Z.Y., 2001. Trilobites from the upper most Torsuqtagh Group (Cambrian–Ordovician), southern Kuruktag area, Xinjiang. Acta Palaeontologica Sinica, 40(3): 330–342 (in Chinese with English abstract).
Liu, H., Liao, Z.W., Zhang, H.Z., Tian, Y.K., Cheng, B., and Yang, S., 2017. Stable isotope ($\delta^{13}C_{ker}$, $\delta^{13}C_{carb}$, $\delta^{18}O_{carb}$) distribution along a Cambrian outcrop section in the eastern Tarim Basin, NW China and its geochemical significance. Geoscience Frontiers, 8(1): 163–170.
Luke, E.F., Paul, B.W., Sara, B.P., Robert, J.N., Sun, Y.D., and Stephen, F.C., 2017. Trilobite extinctions, facies changes and the ROECE carbon isotope excursion at the Cambrian Series 2â 3 boundary, Great Basin, western USA. Palaeogeography, Palaeoclimatology, Palaeoecology. 478: 53–66.
Maloof, A.C., Porter, S.M., Moore, J.L., Dudás, F.Ö., Bowring, S.A., Higgins, J.A., Fike, D.A., and Eddy, M.P., 2010. The earliest Cambrian record of animals and ocean geochemical change. Geological Society of America Bulletin, 122(11–12): 1731–1774.
Maloof, A.C., Schrag, D.P., Crowley, J.L., and Bowring, S.A., 2005. An expanded record of Early Cambrian carbon cycling from the Anti-Atlas Margin, Morocco. Canadian Journal of Earth Sciences, 42(12): 2195–2216.
Marshall, J.D., 1992. Climatic and oceanographic isotopic signals from the carbonate rock record and their preservation. Geological Magazine, 129(2): 143–160.
Meert, J.G., and Santosh, M., 2017. The Columbia supercontinent revisited. Gondwana Research, 50: 67–83.
Miller, J.F., Ethington, R.L., Evans, K.R., Holmer, L.E., Loch, J.D., Popov, L.E., Repetski, J.E., Ripperdan, R.L., and Taylor, J.F., 2006. Proposed stratotype for the base of the highest Cambrian stage at the first appearance datum of Cordylodus andresi, Lawson Cove section, Utah, USA. Palaeoworld, 15(3–4): 384–405.
Montañez, I.P., Osleger, D.A., Banner, J.L., Mack, L.E., and Musgrove, M., 2000. Evolution of the Sr and C isotope composition of Cambrian oceans. GSA today, 10(5): 1–7.
Narbonne, G.M., Kaufman, A.J., and Knoll, A.H., 1994. Integrated chemostratigraphy and biostratigraphy of the Windermere Supergroup, northwestern Canada: Implications for Neoproterozoic correlations and the early evolution of animals. Geological Society of America Bulletin, 106(10): 1281–1292.
Narbonne, G.M., Xiao, S.H., Shields, G.A., and Gehling, J.G., 2012. The Ediacaran Period. In: Gradstein, F.M., Ogg, J.G., Schmitz, M.D., and Ogg, G.M. (eds.), The geologic time

scale, 413–435.

Pang, X.Q., Jia, C.Z., Zhang, K., Li, M.W., Wang, Y.W., Peng, J.W., Li, B.Y., and Chen, J.Q., 2020. The dead line for oil and gas and implication for fossil resource prediction. Earth System Science Data, 12(1): 577–590.

Peng, S., Babcock, L.E., Robison, R.A., Lin, H., Rees, M.N., and Saltzman, M.R., 2004. Global Standard Stratotype-section and Point (GSSP) of the Furongian Series and Paibian Stage (Cambrian). Lethaia, 37(4): 365–379.

Pruss, S.B., Jones, D.S., Fike, D.A., Tosca, N.J., and Wignall, P.B., 2019. Marine anoxia and sedimentary mercury enrichments during the Late Cambrian SPICE event in northern Scotland. Geology, 47(5): 475–478.

Ren, R., Guan, S.W., Zhang, S.C., Wu, L., and Zhang, H.Y., 2020. How did the peripheral subduction drive the Rodinia breakup: Constraints from the Neoproterozoic tectonic process in the northern Tarim Craton. Precambrian Research, 339: 105612.

Ripperdan, R.L., Magaritz, M., and Kirschvink, J.L., 1993. Carbon isotope and magnetic polarity evidence for non-depositional events within the Cambrian–Ordovician boundary section near Dayangcha, Jilin Province, China. Geological Magazine, 130(4): 443–452.

Rothman, D.H., Hayes, J.M., and Summons, R.E., 2003. Dynamics of the Neoproterozoic carbon cycle. Proceedings of the National Academy of Sciences of the United States of America, 100(14): 8124–8129.

Saltzman, M.R., Cowan, C.A., Runkel, A.C., Runnegar, B., Stewart, M.C., and Palmer, A.R., 2004. The Late Cambrian Spice (^{13}C) Event and the Sauk II–SAUK III Regression: New Evidence from Laurentian Basins in Utah, Iowa, and Newfoundland. Journal of Sedimentary Research, 74(3): 366–377.

Saltzman, M.R., Ripperdan, R.L., Brasier, M.D., Lohmann, K.C., Robison, R.A., Chang, W.T., Peng, S.C., Ergaliev, E.K., and Runnegar, B., 2000. A global carbon isotope excursion (SPICE) during the Late Cambrian: Relation to trilobite extinctions, organic–matter burial and sea level. Palaeogeography, Palaeoclimatology, Palaeoecology, 162(3): 211–223.

Saltzman, M.R., Runnegar, B., and Lohmann, K.C., 1998. Carbon isotope stratigraphy of Upper Cambrian (Steptoean Stage) sequences of the eastern Great Basin: Record of a global oceanographic event. Geological Society of America Bulletin, 110(3): 285–297.

Saltzman, M.R., Young, S.A., Kump, L.R., Gill, B.C., Lyons, T.W., and Runnegar, B., 2011. Pulse of atmospheric oxygen during the late Cambrian. Proceedings of the National Academy of Sciences of the United States of America, 108 (10): 3876–3881.

Schmid, S., 2017. Chemostratigraphy and palaeo-environmental characterisation of the Cambrian stratigraphy in the Amadeus Basin, Australia. Chemical Geology, 451: 169–182.

Schobben, M., Ullmann, C.V., Leda, L., Korn, D., Struck, U., Reimold, W.U., Ghaderi, A., Algeo, T.J., and Korte, C., 2016. Discerning primary versus diagenetic signals in carbonate carbon and oxygen isotope records: An example from the Permian–Triassic boundary of Iran. Chemical Geology, 422: 94–107.

Scholz, F., 2018. Identifying oxygen minimum zone-type biogeochemical cycling in Earth history using inorganic geochemical proxies. Earth–Science Reviews, 184: 29–45.

Sial, A., Peralta, S., Gaucher, C., Toselli, A., Ferreira, V., Frei, R., Parada, M., Pimentel, M., and Pereira, N.S., 2013. High-resolution stable isotope stratigraphy of the upper Cambrian and Ordovician in the Argentine Precordillera: Carbon isotope excursions and correlations. Gondwana Research, 24(1): 330–348.

Smith, E.F., Macdonald, F.A., Petach, T.A., Bold, U., and Schrag, D.P., 2016. Integrated stratigraphic, geochemical, and paleontological late Ediacaran to early Cambrian records from southwestern Mongolia. Bulletin, 128(3–4): 442–468.

Su, J., Fang, Y., Ma, S.H., Yang, Y.P., Wei, C.Y., Weng, N., Xu, L., Bi, L.N., Li, H.D., and Lin, K.X., 2020. The excursion of Nitrogen and Carbon isotope in the Lower Cambrian of Tarim Basin: Implication for the transformation of anaerobic and euxinic settling, IOP Conference Series: Earth and Environmental Science, 600(1): 012025.

Ulloa, O., Canfield, D.E., DeLong, E.F., Letelier, R.M., and Stewart, F.J., 2012. Microbial oceanography of anoxic oxygen minimum zones. Proceedings of the National Academy of Sciences of the United States of America, 109(40): 15996–16003.

Wang, P., and Zhu, G.X., 1988. New idea on graptolites, conodonts and trilobites in Cambrian and Ordovician in Queerquek mountain, Xinjiang. Xinjiang Geology, 6(2): 48–53 (in Chinese with English abstract).

Wang, X.L., Hu, W.X., Yao, S.P., Chen, Q., and Xie, X.M., 2011. Carbon and strontium isotopes and global correlation of Cambrian Series 2–Series 3 carbonate rocks in the Keping area of the northwestern Tarim Basin, NW China. Marine and Petroleum Geology, 28(5): 992–1002.

Wang, X.M., Zhang, S.C., He, K., Wang, H.J., Mi, J.K., Su, J., and Ye, Y., 2021. OMZ and euxinic sulfidic environments dominating hydrocarbon generation poential of organic matter 1.4 billion years ago. Chinese Science Bulletin, 66(23): 3005–3017 (in Chinese with English abstract).

Woods, M.A., Wilby, P.R., Leng, M.J., Rushton, A.W.A., and Williams, M., 2011. The furongian (late Cambrian) steptoean positive carbon isotope excursion (SPICE) in Avalonia. Journal of the Geological Society, 168(4): 851–862.

Xiao, S.H., Bao, H.M., Wang, H.F., Kaufman, A.J., Zhou, C.M., Li, G.X., Yuan, X.L., and Ling, H.F., 2004. The Neoproterozoic Quruqtagh Group in eastern Chinese Tianshan: Evidence for a post–Marinoan glaciation. Precambrian Research, 130(1–4): 1–26.

Xiong, J.F., Yu, T.X., Cao, Z.C., Zhao, M., Fan, H.Y., and Wu, T., 2011. New advances in Cambrian biostratigraphy of the covered area of the Tarim Basin. Journal of Stratigraphy, 35 (4): 419–430 (in Chinese with English abstract).

Yan, L., Yang, M., Zhang, J.L., Cao, Y.H., Du, D.D., Wang, S., Xu, Z.H., Li, H.H., and Zhao, Y.M., 2020. Distribution of Cambrian source rocks and evaluation and optimization of favorable zones in East Tarim Basin. Natural Gas Geoscience, 31(5): 667–674 (in Chinese with English abstract).

Yang, S.P., 1994. Cambrian–Ordovician trace fossils from Kuruktag MT., north–eastern part of Tarim Basin. Geoscience, 8(4): 371–371 (in Chinese with English abstract).

Yang, X.Q., Li, Z., Gao, B., and Zhou, Y.Q., 2021. The Cambrian Drumian carbon isotope excursion (DICE) in the Keping area of the northwestern Tarim Basin, NW China. Palaeogeography, Palaeoclimatology, Palaeoecology, 571: 110385.

Yao, C.Y., Ma, D.S., Ding, H.F., and Zhang, X.Y., 2011. Early cambrian carbon isotope stratigraphy in the tarim basin and a correlation with the yangtze platform. Chinese Journal of Geochemistry, 30(3): 382–390.

Yao, J.X., Xiao, S.H., Yin, L.M., Li, G.X., and Yuan, X.L., 2005. Basal Cambrian microfossils from the Yurtus and Xishanblaq formations (Tarim, north–west China): Systematic revision and biostratigraphic correlation of *Micrhystridium*–like acritarchs. Palaeontology, 48(4): 687–708.

Ye, Y.T., Wang, H.J., Wang, X.M., Wu, C.D., Canfield, D.E., and Zhang, S.C., 2022. Application of Cd as a paleo–environment indicator. Palaeogeography, Palaeoclimatology, Palaeoecology, 585: 110749.

Zhai, M.G., 2013. The main old lands in China and assembly of Chinese unified continent. Science in China Series D: Earth Sciences, 56(11): 1829–1852.

Zhang, S.G., 1983. Early Cambrian archaeocyathids from Kuruktag, Xinjiang. Acta Palaeontologica Sinica, 1(22): 9–20 (in Chinese with English abstract).

Zhang, S.C., and Huang, H.P., 2005. Geochemistry of Palaeozoic marine petroleum from the Tarim Basin, NW China: Part 1. Oil family classification. Organic Geochemistry, 36(8): 1204–1214.

Zhang, S.C., Wang, X.M., Wang, H.J., Bjerrum, C.J., Hammarlund, E.U., Costa, M.M., Connelly, J.N., Zhang, B.M., Su, J., and Canfield, D.E., 2016. Sufficient oxygen for animal respiration 1,400 million years ago. Proceedings of the

National Academy of Sciences of the United States of America, 113(7): 1731–1736.
Zhang, S.C., Zhang, B.M., and Wang, F.Y., 2004. Oil accumulation history in Tadong–2 oil reservoir in Tarim Basin, NW China—A case study of oil stability and cracking. Petroleum Exploration and Development, 31(6): 25–30.
Zhang, T.R., 1990. Succession of the Cambrian trilobite faunas in Kuruktag. Xinjiang Geology, 2(8): 185–192 (in Chinese with English abstract).
Zhang, T., Li, Y.F., Fan, T.L., Lash, G., Gao, Z.Q., and Fan, Q., 2020a. Marine carbon and sulfur cycling across the Ediacaran–Cambrian boundary in Tarim Block and its implications for paleoenvironmental changes. Palaeogeography, Palaeoclimatology, Palaeoecology, 560: 110011.
Zhang, X.L., 2021. Marine refractory dissolved organic carbon and transgressive black shales. Chinese Science Bulletin, doi: 10.1360/TB–2021–0613 (in Chinese with English abstract).
Zhang, X.L., and Shu, D.G., 2021. Current understanding on the Cambrian Explosion: Questions and answers. PalZ: 1–20.
Zhang, X.L., Zhou, X., and Hu, D.P., 2020b. High-resolution paired carbon isotopic records from the Meishucun section in South China: Implications for carbon cycling and environmental changes during the Ediacaran–Cambrian transition. Precambrian Research, 337: 105561.
Zhang, Y.G., Yang, T., Hohl, S.V., Zhu, B., He, T.C., Pan, W.Q., Chen, Y.Q., Yao, X.Z., and Jiang, S.Y., 2020c. Seawater carbon and strontium isotope variations through the late Ediacaran to late Cambrian in the Tarim Basin. Precambrian Research, 345: 105769.
Zhang, Z.Y., Zhu, G.Y., Wu, G.H., Li, T.T., Feng, X.Q., and Jing, Y.H., 2022. Carbon isotopic chemostratigraphy of the Ediacaran–Cambrian successions in the northwestern Tarim Craton, NW China: Correlations with Gondwana supercontinent. Global and Planetary Change, 208: 103702.
Zhao, F.C., Zhu, M.Y., and Hu, S.X., 2010. Community structure and composition of the Cambrian Chengjiang biota. Science in China Series D: Earth Sciences, 53(12): 1784–1799.
Zhao, G.C., Wang, Y.J., Huang, B.C., Dong, Y.P., Li, S.Z., Zhang, G.W., and Yu, S., 2018. Geological reconstructions of the East Asian blocks: From the breakup of Rodinia to the assembly of Pangea. Earth–Science Reviews, 186: 262–286.
Zhao, Y.L., Yuan, J.L., Guo, Q.J., Peng, J., Yin, L.M., Yang, X.L., Wang, C.J., and Sun, H.J., 2014. Comments on some important issues concerning the establishment of a GSSP for Cambrian Stage 5. Geologiska Freningen I Stockholm Frhandlingar, 136(1): 333–336.
Zhao, Z.J., Luo, J.H., Zhang, Y.B., Wu, X.N., and Pan, W.Q., 2011. Lithofacies paleogeography of Cambrian sequences in the Tarim Basin. Acta Petrolei Sinica, 32(6): 937–948 (in Chinese with English abstract).
Zhou, Z.Y., and Chen, P.J., 1990. Biostratigraphy and Geological Evolution of the Tarim Basin. Beijing: Science Press.
Zhu, B., Yang, T., Wang, J., Chen, X., Pan, W.Q., and Chen, Y.Q., 2021a. Multiple controls on the paleoenvironment of the early Cambrian black shale–chert in the northwest Tarim Basin, NW China: Trace element, iron speciation and Mo isotopic evidence. Marine and Petroleum Geology, 136: 105434.
Zhu, C.F., 2007. New materials of Cambrian small shell fossils from Kuruketage, Xinjiang The 24th Annual Conference of Palaeontological Society of China, Pingyi, Shandong, 8 (in Chinese).
Zhu, G.Y., Chen, F.R., Wang, M., Zhang, Z.Y., Ren, R., and Wu, L., 2018. Discovery of the lower Cambrian high–quality source rocks and deep oil and gas exploration potential in the Tarim Basin, China. AAPG Bulletin, 102(10): 2123–2151.
Zhu, G.Y., Li, T.T., Zhao, K., Li, C., Cheng, M., Chen, W.Y., Yan, H.H., Zhang, Z.Y., and Algeo, T.J., 2021b. Mo isotope records from Lower Cambrian black shales, northwestern Tarim Basin (China): Implications for the early Cambrian ocean. Geological Society of America Bulletin, 134(1–2): 3–14.
Zhu, M.Y., Zhang, J.M., Li, G.X., and Yang, A.H., 2004a. Evolution of C isotopes in the Cambrian of China: implications for Cambrian subdivision and trilobite mass extinctions. Geobios, 37(2): 287–301.
Zhu, M.Y., Sun, Z.X., Yang, A.H., Yuan, J.L., Li, G.X., Zhou, Z.Q., and Zhang, J.M., 2021c. Lithostratigraphic subdivision and correlation of the Cambrian in China. Journal of Stratigraphy, 45(3): 223–249 (in Chinese with English abstract).
Zhu, M.Y., Yang, A.H., Yuan, J.L., Li, G.X., Zhang, J.M., Zhao, F.C., Ahn, S.Y., and Miao, L.Y., 2019. Cambrian integrative stratigraphy and timescale of China. Science China Earth Sciences, 62(1): 25–60.
Zhu, M.Y., Babcock, L.E., and Peng, S.C., 2006. Advances in Cambrian stratigraphy and paleontology: integrating correlation techniques, paleobiology, taphonomy and paleoenvironmental reconstruction. Palaeoworld, 15(3): 217–222.
Zhu, M.Y., Zhang, J.M., Li, G.X., and Yang, A.H., 2004b. Evolution of C isotopes in the Cambrian of China: implications for Cambrian subdivision and trilobite mass extinctions. Geobios, 37(2): 287–301.
Zhu, Z.L., and Lin, H.L., 1983. Some Early Cambrian trilobites from the Xidashan Formation of Kuruktag, Xinjiang. Acta Palaeontologica Sinica, 22(1): 21–32 (in Chinese with English abstract).
Zou, C.N., Du, J.H., Xu, C.C., Wang, Z.C., Zhang, B.M., Wei, G.Q., Wang, T.S., Yao, G.S., Deng, S.H., and Liu J.J., 2014. Formation, distribution, resource potential, and discovery of Sinian–Cambrian giant gas field, Sichuan Basin, SW China. Petroleum Exploration and Development, 41(3): 306–325.
Zuo, J.X., Peng, S.C., Qi, Y.P., Zhu, X.J., Bagnoli, G., and Fang, H.B., 2018. Carbon–isotope excursions recorded in the Cambrian system, South China: Implications for mass extinctions and sea–level fluctuations. Journal of Earth Science, 29(3): 479–491.

About the first author

WANG Huajian, male, born in 1984 in Jining, Shandong Province; Doctor; Senior engineer; graduated from the Institute of High Energy Physics of the Chinese Academy of Sciences in 2011. He is now mainly engaged in source rock geochemistry, petroleum geology and Precambrian geology. E-mail: wanghuajian@petrochina.com.cn; phone: 010-83595538.

About the corresponding author

ZHANG Shuichang, male, born in 1961 in Yuzhou, Henan Province; Doctor; Professor; graduated from the Chinese University of Geosciences (Beijing) in 1991. He is now mainly engaged in organic geochemistry and petroleum geology. E-mail: sczhang@petrochina.com.cn; phone: 010-83598360.